The Yarlung Suture Mélange, Lopu Range, Southern Tibet: Provenance of Sandstone Blocks and Transition from Oceanic Subduction to Continental Collision

Kathryn Metcalf[1*] and Paul Kapp[1]

[1]Department of Geosciences, University of Arizona, Tucson, AZ, USA

[*]Corresponding author. Email: kmetcalf@email.arizona.edu

Abstract

With the aim of better understanding the history of ocean closure and suturing between India and Asia, we conducted a geologic investigation of a siliciclastic matrix tectonic mélange within the western Yarlung suture zone of southern Tibet (Lopu Range region, ~50 km northwest of Saga). The siliciclastic matrix mélange includes abundant blocks of ocean plate stratigraphy and sparse blocks of sandstone. Metapelite and metabasite blocks in the mélange exhibit lower greenschist facies mineral assemblages, indicating that they were not deeply subducted. We obtained detrital zircon U-Pb geochronologic and sandstone petrographic data from sandstone blocks in the mélange and sandstone beds from Tethyan Himalaya strata exposed to the south of the suture. The sandstones from both units are all similar in U-Pb detrital zircon age spectra and petrography to the nearby Tethyan Cretaceous – Paleocene Sangdanlin section, which records the earliest appearance (at ~59 Ma) of arc-affinity strata deposited conformably on Indian-affinity strata. Two Paleocene sandstones, one of which is a schistose block incorporated in the siliciclastic matrix mélange, yielded indistinguishable maximum depositional ages of ~59 Ma. Mesozoic Asian-affinity sandstone blocks previously documented in the siliciclastic matrix mélange 200-500 km along strike to the east are notably absent in the Lopu Range region. We documented a gradational transition in structural style from the block-in-matrix mélange in the northeast to the south-vergent Tethyan thrust belt in the southwest. Blocks of Tethyan Himalaya strata increase in

size and the volumetric proportion of matrix decreases from northeast to southwest. We conclude that no arc-affinity sandstone blocks were incorporated into the subduction complex until India-Asia collision at ~59 Ma when the Xigaze forearc basin became overfilled and Tethyan Himalaya strata entered the trench. As collision progressed, there was a gradual transition in structural style from block-in-matrix mélange formation to imbricate-style thrust belt formation.

Keywords: subduction, mélange, accretion, suture zone, southern Tibet

1. Introduction

Many studies in the Yarlung Suture Zone (YSZ) have focused on the timing of India-Asia collision, but the dynamics of the trench during Neotethyan oceanic subduction and the transition to continental collision remain poorly understood. The subduction complex in the YSZ along the Yarlung River is dominated by ocean plate stratigraphy accreted during oceanic subduction. We use the term subduction complex to encompass accretionary prisms (deformed ocean plate stratigraphy) and frontal prisms (deformed upper plate basement) found in accretionary and erosive margins respectively (von Huene et al., 2004). Ocean plate stratigraphy is defined as volcanic and sedimentary oceanic upper crust, including pillow basalts, abyssal cherts, seamounts, and terrigenous trench fill (Wahrhaftig, 1984; Isozaki et al., 1990; Wakita and Metcalfe, 2005; Kusky et al., 2013; Wakita, 2015). In all well-dated subduction complexes, the age of accretion youngs toward the trench (Kusky et al., 2013 and references therein), such that changes in provenance and volume of material accreting at the trench can be reconstructed through time. Generally, thicker trench fill creates an accretionary subduction complex composed mostly of ocean plate stratigraphy while thinner trench fill leads to an erosive subduction complex marked by frontal erosion and/or basal erosion of the margin, forearc subsidence, and inboard migration of the forearc and arc (von Huene and Scholl, 1991; Clift and Vannucchi, 2004; Stern, 2011).

Trench fill thickness is related to both the sediment flux from the upper plate and the subduction rate (Clift and Vannucchi, 2004).

From north to south across the Yarlung Suture Zone in southern Tibet, the following rock assemblages are exposed: (Fig. 1), the Mesozoic to Paleogene Gangdese continental margin arc, the late Cretaceous to Eocene Xigaze forearc basin, the early Cretaceous Xigaze ophiolite belt, the subduction complex, and Indian-affinity Tethyan Himalaya Sequence strata. With the exception of local amphibolite in the ophiolite belt, a few local outcrops of blueschist in the siliciclastic matrix mélange (Ding et al., 2005; Li et al., 2007; Wang et al., 2017), and rocks exhumed by doming and/or normal faulting, the suture zone is regionally metamorphosed to lower greenschist facies (ophiolite belt Burg and Chen, 1984; Tethyan Himalaya strata Burg and Chen, 1984; Burg et al., 1987; Xigaze forearc basin Dürr, 1996; ophiolite belt Huot et al., 2002; Dupuis et al., 2005a; Dupuis et al., 2005b; Cai et al., 2012). The siliciclastic matrix mélange within the subduction complex has long been interpreted to have formed by accretion of ocean plate stratigraphy beneath the ophiolite belt and as the southernmost Asian unit (Shackleton, 1981; Tapponnier et al., 1981; Searle et al., 1987; Cai et al., 2012). Alternatively, Aitchison et al. (Aitchison et al., 2000) interpreted the siliclastic matrix mélange as telescoped Tethyan Himalaya strata, the northernmost part of the Tethyan thrust belt south of the Yarlung Suture, and introduced the locally exposed Bainang terrane as the subduction complex. Collision between the Tethyan Himalaya and an arc is constrained to 60-65 Ma based on the youngest fossils in the subduction complex (Tapponnier et al., 1981; Burg and Chen, 1984; Burg et al., 1985; Liu and Aitchison, 2002) and ~60 Ma based on stratigraphic dating of the earliest arc-

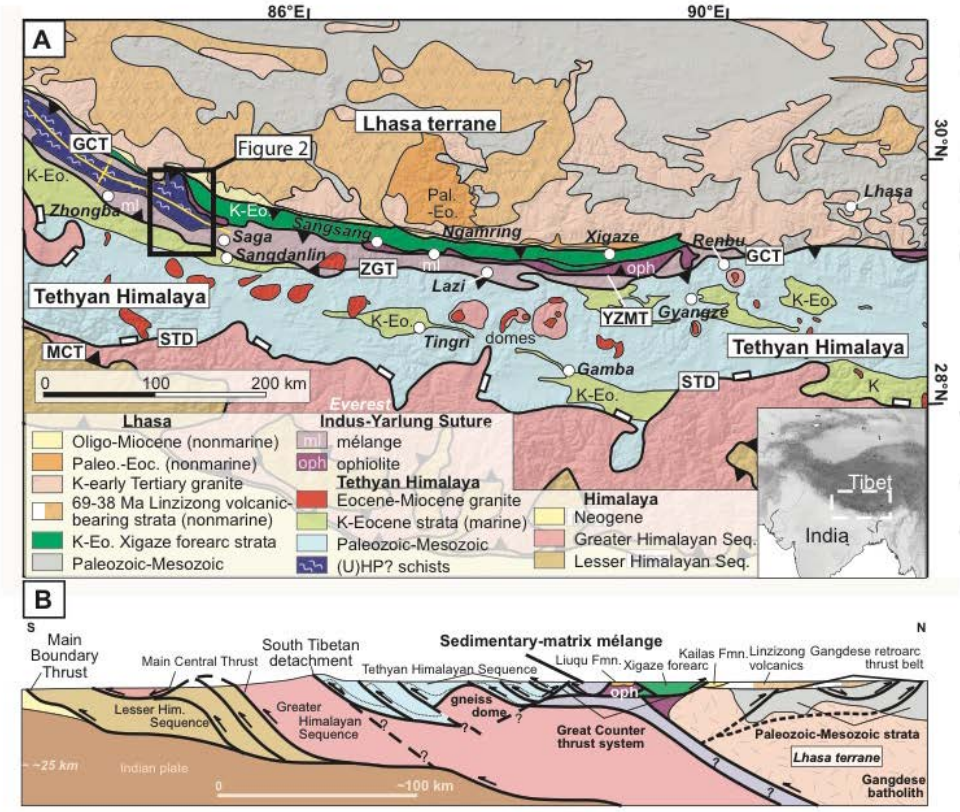

Figure 1

Figure 1. (a) Simplified regional geologic map. The siliciclastic matrix mélange (light purple) is continuously exposed from Xigaze in the east past Zhongba in the west. GCT: Great Counter Thrust, MCT: Main Central Thrust, STD: South Tibetan Detachment, YZMT: Yarlung Zangbo Mantle Thrust, ZGT: Zhongba-Gyangze Thrust. (b) Simplified cross section from the Lhasa terrane across the Yarlung Suture Zone and the Himalayan thrust belt. Modified after Orme et al. (2015).

affinity strata deposited on Indian-affinity strata (~64 Ma Ding et al., 2005; ~57 Ma Aitchison et al., 2007; ~54 Ma Wang et al., 2011; 58-60 Ma DeCelles et al., 2014; ~60 Ma Wu et al., 2014; ~59 Ma Hu et al., 2015a). Tectonic models interpret Paleocene collision between 1) the Indian passive margin and an intraoceanic arc followed by later collision with Asia, 2) the Indian passive margin and the Gangdese arc on the southern margin of Asia, or 3) the Tethyan Himalaya microcontinent and the Gangdese arc on the southern margin of Asia. See Aitchison et al. (2007) and Hu et al. (2016) for reviews of the various collision scenarios and the evidence on which they are based. For now, we will refer to the Paleocene collision as India-arc collision and return to the tectonic models in the discussion. This study is focused on how the subduction complex responded compositionally and structurally to the India-arc collision along with its implications for the setting in which it formed and what collided with India during the Paleocene.

We collected sandstones from the subduction complex and Tethyan Himalaya strata for U-Pb detrital zircon dating to determine the relative input of upper-plate- and lower-plate-derived sediments into the trench through time. The Lopu Range ~50 km northwest of Saga (Fig. 1), is an ideal location to explore for potential inputs to the trench because the Cretaceous to Paleocene stratigraphy of the Xigaze forearc basin and the Tethyan Himalaya are well-studied in the area and have been shown to record India-arc collision (Ding et al., 2005; Aitchison et al., 2007; Wang et al., 2011; DeCelles et al., 2014; Wu et al., 2014; Orme et al., 2015; Hu et al., 2015a; Hu et al., 2015b; Baxter et al., 2016). Our data indicate that no sandstone was incorporated into the subduction complex until the initiation of India-arc collision at ~59 Ma. Despite little or no record of trench fill in the field area, a subduction complex developed by accretion of ocean plate stratigraphy (pelagic sediments, seamounts, basalts, and metabasites) during at least Cretaceous to Paleocene time. When the first Tethyan stratigraphy entered the trench, Tethyan- and arc-affinity

sandstone blocks were incorporated into the subduction complex. As thicker, distal Tethyan Himalaya strata entered the trench, deformation changed in style from block-in-matrix mélange to imbricate thrusting of coherent sheets of Tethyan Himalaya stratigraphy.

2. Geologic Setting

The Gangdese magmatic arc developed along the southern margin of the Lhasa terrane and is composed predominantly of granodiorite and the volcanic-bearing Paleocene – Eocene Linzizong Formation. Arc-type magmatism initiated as early as late Triassic or early Jurassic time (Chu et al., 2006; Ji et al., 2009; Zhu et al., 2011; Guo et al., 2013; Kang et al., 2014; Meng et al., 2016). The Gangdese magmatic arc shows well resolved magmatic peaks at 103-80 Ma and 65-45 Ma and an intervening lull at 80-69 Ma (Chu et al., 2006; Wen et al., 2008; Ji et al., 2009; Lee et al., 2009; Hu et al., 2012). The southernmost Gangdese arc is overlain in buttress unconformity by the Oligocene-Miocene Kailas Formation (Heim and Gansser, 1939; Aitchison et al., 2002; DeCelles et al., 2011; Leary et al., 2016a), which everywhere along strike is bound to the south by the northernmost strand of the north-verging, south-dipping ~19-13 Ma Great Counter Thrust system (GCT), also known as the Renbu-Zedong Thrust (RZT) east of Xigaze (Heim and Gansser, 1939; Burg et al., 1987; Ratschbacher et al., 1994; Yin et al., 1994; Quidelleur et al., 1997; Yin et al., 1999; Yin and Harrison, 2000; Murphy and Yin, 2003).

The Xigaze forearc basin is exposed in an east-west trending synclinorium to the south of the Kailas Formation in the hanging wall of the GCT. It was filled with strata of the Lower Cretaceous to Coniacian Xigaze Group and the Santonian to Eocene Tso-Jiangding Group in a mostly marine setting along the southern margin of Asia (Liu et al., 1988; Einsele et al., 1994; Dürr, 1996; Ding et al., 2005; Wang et al., 2012; Orme et al., 2015; Orme and Laskowski, 2016). The basal forearc basin has been interpreted to locally be in depositional contact with underlying

ophiolite belt units (Marcoux et al., 1982; Girardeau et al., 1984; Wang et al., 2012; An et al., 2014; Huang et al., 2015; Orme and Laskowski, 2016), but in most places is bound by faults associated with the GCT system. The correlation of Xigaze forearc basin stratigraphy with the strata deposited on the ophiolite is disputed (Aitchison et al., 2000; Ziabrev et al., 2003). Deep-marine turbidites of the Xigaze Group transition to shallow marine and fluvio-deltaic facies upsection in the Tso-Jiangding Group (Ding et al., 2005; Wang et al., 2012; Orme et al., 2015; Orme and Laskowski, 2016). Both sandstone petrography and detrital zircon geochronology suggest a Gangdese arc and Lhasa terrane provenance for the forearc basin (Dürr, 1996; Wu et al., 2010; An et al., 2014; Dai et al., 2015; Orme et al., 2015; Hu et al., 2015b; Orme and Laskowski, 2016). The youngest preserved strata of the Xigaze forearc basin are exposed northeast and northwest of the Lopu Range (Fig. 2) and were deposited from ~88 to ~54 Ma (Ding et al., 2005; Orme et al., 2015) and ~74 to ~54 (Hu et al., 2015b) respectively. Northeast of the Lopu Range, Orme et al. (2015) documented the transition of depositional environments from distal Upper Cretaceous turbidite fan deposits to fluvial deposits at 58-54 Ma as the forearc basin filled. Northwest of the Lopu Range, Hu et al. (2015b) document the transition of depositional environments from shelfal to fan-delta. The sandstone petrography also changes upsection from a transitional arc provenance in Cretaceous strata to a dissected arc (Orme et al., 2015) and recycled orogen (Hu et al., 2015b) provenance in Paleogene strata.

Late Jurassic and early Cretaceous ophiolite massifs and ophiolitic mélanges are present along much of the YSZ. Ophiolite massifs are distributed along the ophiolite belt within ophiolitic mélanges composed of chert and serpentinitized mafic-ultramafic blocks tectonized in a serpentinite matrix. Their geochemical signatures are heterogeneous, ranging from back-arc-

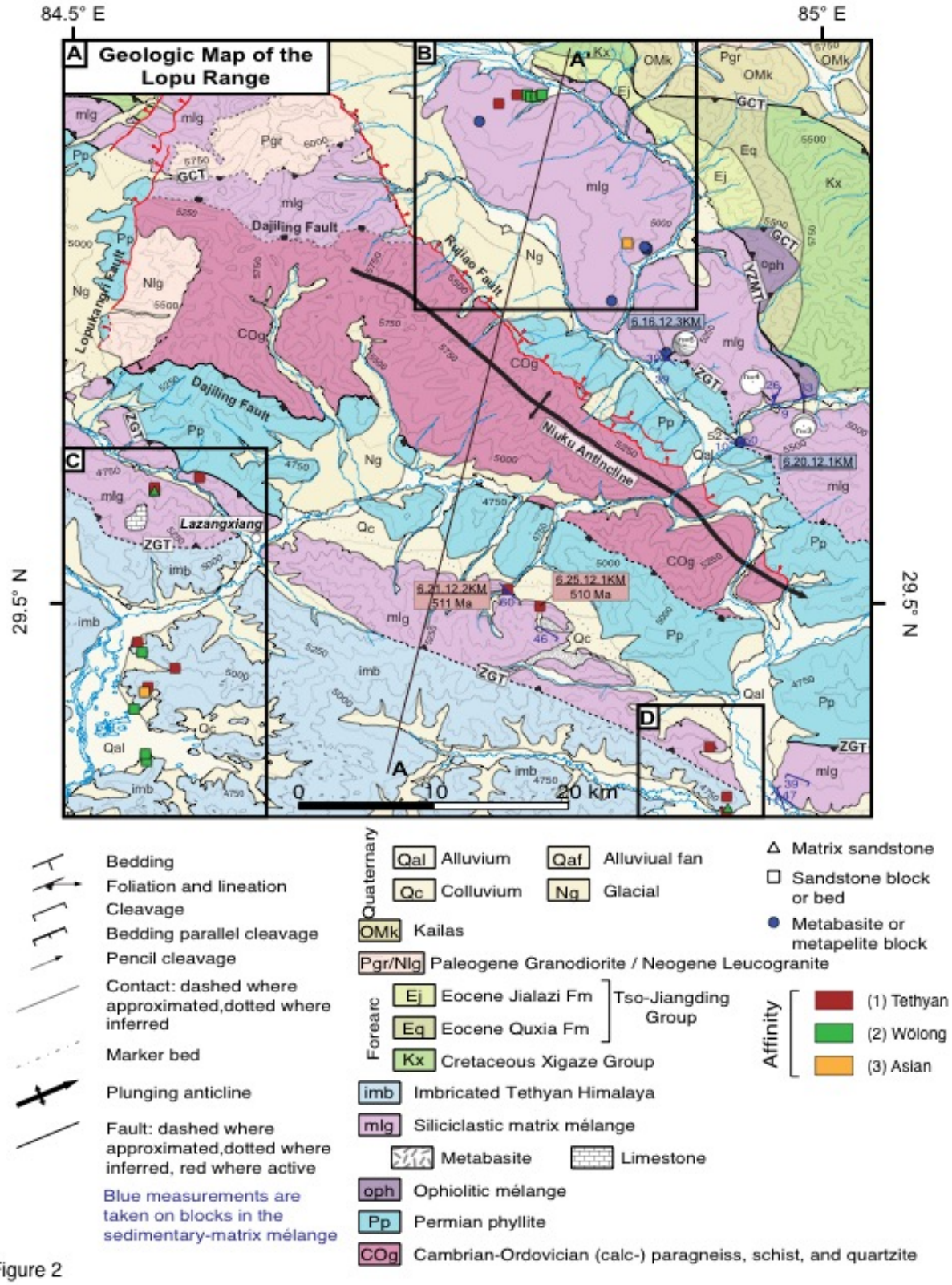

Figure 2

144

145

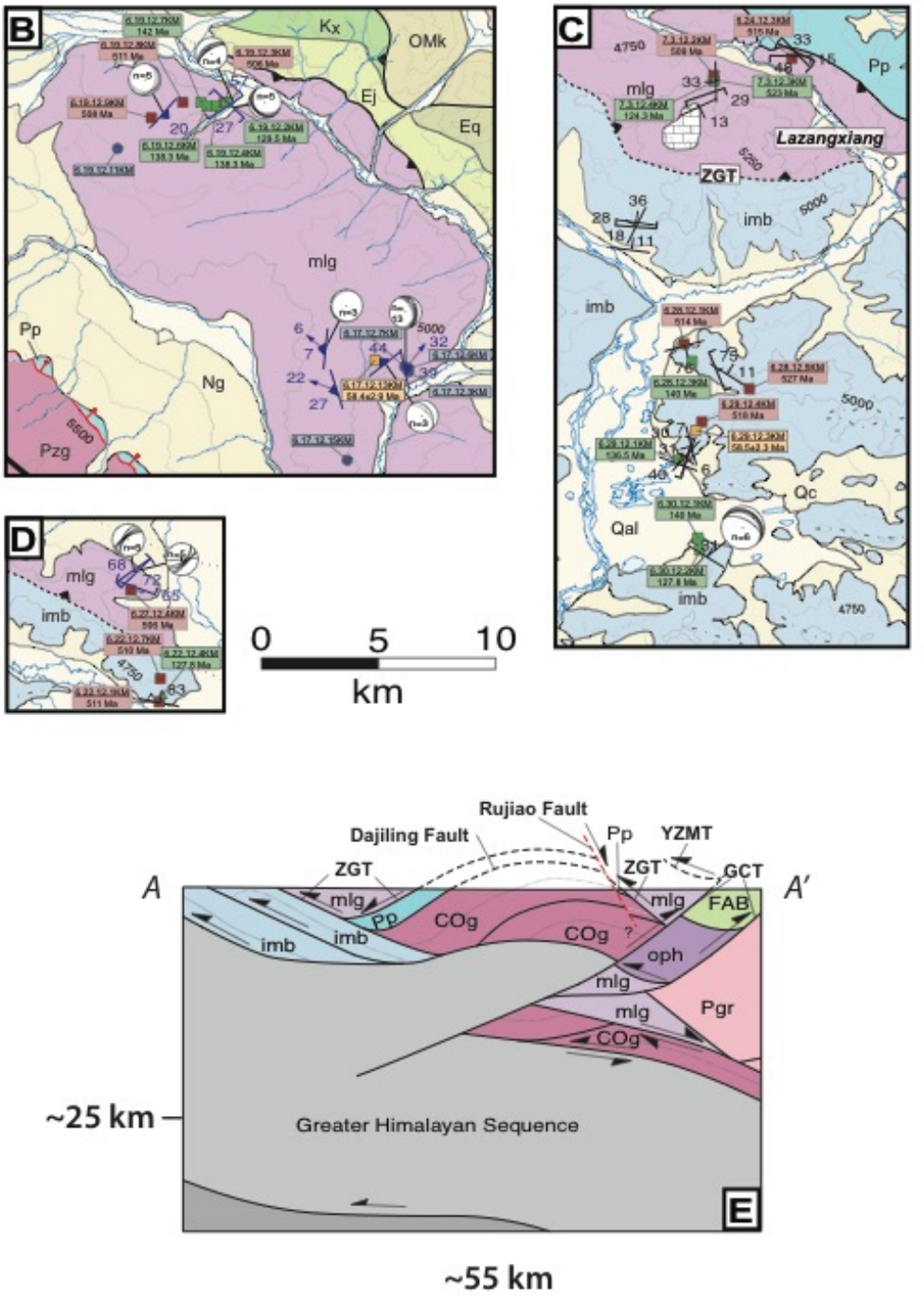
B
Kx
OMk
Ej
Eq
mlg
Pp
Ng
Pzg
5800
5000
C
Pp
mlg
Lazangxiang
ZGT
imb
5000
imb
Qc
Qal
imb
4750
D
mlg
imb
4750
0
5
10
km
A
A′
Rujiao Fault
Dajiling Fault
Pp
YZMT
ZGT
ZGT
GCT
mlg
mlg
FAB
Pp
COg
COg
imb
imb
oph
mlg
Pgr
mlg
COg
~25 km
Greater Himalayan Sequence
E
~55 km

Figure 2

147 Figure 2. Geologic map of the Lopu Range. After Orme et al. (2015), Laskowski et al. (2016),

148 Laskowski et al. (2017), and our own field observations. GCT: Great Counter Thrust, YZMT:

149 Yarlung Zangbo Mantle Thrust, ZGT: Zhongba-Gyangze Thrust.

basin and island arc, with some shoshonitic and boninitic geochemistries, to normal mid-ocean ridge basalt (N-MORB) and ocean island basalt (OIB) (Hébert et al., 2012 and references therein). Geochronological ages cluster around 165-150 Ma and 135-120 Ma, but even the same massif may have units with different ages and variable geochemical signatures (Hébert et al., 2012). The range of ages and geochemical signatures in the ophiolite and ophiolitic mélanges are consistent with their generation within a supra-subduction zone setting (Hébert et al., 2012; Dai et al., 2013). The ophiolite crust is thin (<3 km) compared to typical oceanic crust, consistent with extensional dismemberment along a magma-poor oceanic spreading center (Nicolas et al., 1981; Girardeau et al., 1984). A 127 Ma amphibolite metamorphic sole separates the ophiolite from underlying ophiolitic mélange near Xigaze and is dismembered within the ophiolitic mélange near Saga (Guilmette et al., 2009; Guilmette et al., 2012) (Fig. 1). Whether the ophiolite belt developed proximal or distal to Asia and whether it accreted to India or Asia first has been debated along with the age of continental collision. Paleomagnetic data from Barremian-Aptian radiolarian chert and sandstone strata deposited on the ophiolite suggest that the ophiolite developed proximal to the southern margin of Asia during early Cretaceous time (Huang et al., 2015). This is contrary to previous paleomagnetic work which determined they were deposited at an equatorial paleolatitude (Abrajevitch et al., 2005) and not conformable with the Xigaze forearc basin strata (Aitchison et al., 2000; Ziabrev et al., 2003). Mantle sequences were rotated along detachment faults after magmatic accretion and before forearc sedimentation, suggesting that the ophiolite extended rapidly shortly before forearc basin deposition (Aitchison et al., 2000; Dai et al., 2013; Maffione et al., 2015). The geochemistry and structure of the ophiolite belt suggest that it formed in a forearc setting, but a variety of models continue to debate whether 1) the ophiolite is the basement to the Xigaze forearc basin and collided with India at the onset of India-Asia collision or 2) the ophiolite

developed in the forearc of an intraoceanic arc which collided with India prior to India-Asia collision. Any ties between Asia and the subduction complex would shed light on this debate.

The Yarlung Zangbo Mantle Thrust (YZMT) places ophiolite belt units southward on siliciclastic matrix mélange or Tethyan Himalaya strata, with local red radiolarian chert and/or strata of the synkinemetic Liuqu conglomerate (Paleogene Davis et al., 2002; Eocene Wang et al., 2010; Oligo-Miocene Wei et al., 2011; Oligo-Miocene Li et al., 2015a; 19-20 Ma Leary et al., 2016b) in the hanging wall or footwall (Tapponnier et al., 1981; Burg and Chen, 1984; Girardeau et al., 1984; Burg et al., 1987; Ratschbacher et al., 1994; Ding et al., 2005). The siliciclastic matrix mélange was originally described as "wildflysch with exotic blocks" (Tapponnier et al., 1981; Burg and Chen, 1984; Burg et al., 1985; Burg et al., 1987) and is also known as the Yamdrok mélange (Searle et al., 1987), mud-matrix mélange (Wang et al., 2011), Pomunong mélange (Cai et al., 2012), Renbu mélange (Li et al., 2015b), Xiukang mélange (XBGMR, 1979; Yin and Sun, 1988; An et al., 2017), or sedimentary-matrix mélange (Ding et al., 2005; Wang et al., 2017). There has been some confusion in the literature about the boundaries of the siliciclastic matrix mélange unit, and many definitions of the unit have also included imbricated radiolarian chert and/or deformed Tethyan Himalaya strata. Tapponnier et al. (1981) recognized two distinct flysch units: Cretaceous "wildflysch with exotic blocks" (siliciclastic matrix mélange) to the north and "Triassic flysch" (deformed Triassic Tethyan strata) to the south. These were considered jointly by Shackleton (1981) as the "sedimentary mélange," but separately by Searle et al. (1987) who referred to the wildflysch as the Yamdrok mélange. Aitchison et al. (2000) identified the Bainang terrane, analogous to the locally exposed "infra-ophiolitic thrust sheets of radiolarites" described by Burg et al. (1984) and Upper Jurassic – Lower Cretaceous red radiolarites described by Girardeau et al. (1984), as the subduction complex. The Yamdrok mélange is described as block-

196 in-matrix mélange to broken formation of mostly Indian passive margin with a few “more distal”
197 blocks, similar to the sedimentary mélange of Shackleton (1981) and reinterpreted as telescoped
198 Indian passive margin strata related to India-arc collision (Aitchison et al., 2000). Subsequent
199 publications interpreted that Aitchison et al. (2000) renamed the Yamdrok mélange as the Bainang
200 terrane and included in this unit both the imbricated radiolarites and siliciclastic matrix mélange
201 units. (e.g. Dupuis et al., 2005b; Dupuis et al., 2006; Guilmette et al., 2009). Cai et al. (2012)
202 identified the imbricated radiolarites (the Bainang terrane) as the Tangga mélange and the
203 siliclastic matrix mélange (the Yamdrok mélange) as the Pomunong mélange. The Renbu mélange
204 (Li et al., 2015b), Xiukang mélange (XBGMR, 1979; Yin and Sun, 1988; An et al., 2017), and
205 sedimentary-matrix mélange (Ding et al., 2005; Wang et al., 2017) all refer to the same unit as the
206 Yamdrok mélange from Searle et al. (1987). This disambiguation is important when assessing
207 published descriptions of the siliciclastic matrix mélange. We define the siliciclastic matrix
208 mélange as separate from the imbricated radiolarites and deformed Tethyan strata. Although the
209 mélange contains blocks of Tethyan strata, it is mostly composed of blocks of ocean plate
210 stratigraphy.

211 Published descriptions of the siliciclastic matrix mélange (excluding references to the
212 imbricated radiolarites and deformed Tethyan Himalaya strata) indicate a purely block-in-matrix
213 structural fabric. No outcrops of imbricate ocean plate stratigraphy have been documented within
214 the mélange unit. The siliclastic matrix mélange includes blocks of basalt, metabasite, chert,
215 marine limestone, sandstone, and shale in a sandstone and shale matrix (Shackleton, 1981;
216 Tapponnier et al., 1981; Searle et al., 1987; Dupuis et al., 2005b; Dupuis et al., 2006; Cai et al.,
217 2012; Li et al., 2015b; An et al., 2017; Wang et al., 2017). Kilometer-scale blocks of marine
218 limestone in the mélange and Tethyan Himalaya strata contain Permian to earliest Triassic fossils

(Tapponnier et al., 1981; Jin et al., 2015) and are interpreted to be olistostromal blocks derived from the passive margin of India (Liu and Einsele, 1996; Jin et al., 2015), but fossils as young as latest Cretaceous to late Paleocene are found in the mélange blocks and matrix (Tapponnier et al., 1981; Burg and Chen, 1984; Burg et al., 1985; Liu and Aitchison, 2002). Basalt blocks from the mélange exhibit geochemical characteristics similar to seamounts such as the Réunion hotspot track (Dupuis et al., 2005b). While blueschist is well-documented in the Indus Suture Zone in the northwestern Himalaya, only local outcrops of blueschist have been documented in the siliciclastic matrix mélange (Ding et al., 2005; Li et al., 2007; Wang et al., 2017). Shackleton (1981) described the southernmost part of the mélange as sedimentary in origin, although this may be in reference to the deformed Tethyan strata to the south that is included in the "sedimentary mélange", while Searle et al. (1987) argued for a clearly tectonic origin ~100 km west of Xigaze, consistent with documentation of foliation, lineation, and S-C fabrics in the siliclastic matrix (Burg and Chen, 1984; Cai et al., 2012). The siliciclastic matrix mélange has long been interpreted as a subduction complex formed by subduction-accretion processes during northward subduction of the Neotethyan oceanic slab (Shackleton, 1981; Tapponnier et al., 1981; Searle et al., 1987; Cai et al., 2012). The Bainang terrane, which has also been interpreted as a subduction complex (Aitchison et al., 2000), is not exposed in the Lopu Range area, so we focus here on the siliciclastic matrix mélange.

In the Sangsang area, ~200 km east of the Lopu Range (Fig. 1), two sandstone matrix and two sandstone block samples from the siliciclastic matrix mélange have maximum depositional ages of ~87 Ma and contain Mesozoic and older zircon populations interpreted to be derived from the Lhasa terrane and Gangdese magmatic arc (Wang et al., 2017). In the Ngamring area, ~250 km east of the Lopu Range (Fig. 1), the siliciclastic matrix mélange contains sandstone blocks with

Paleozoic and older detrital zircon age populations as well as Mesozoic populations that share the same age peaks and lulls with the Gangdese magmatic arc and Xigaze forearc basin (Cai et al., 2012). The maximum depositional ages of the Ngamring mélange sandstone blocks range from 85 Ma to 200 Ma with individual grains as young as 71 Ma, and the sandstone petrography falls in the recycled orogen field, suggesting that the sandstone blocks were derived from the forearc basin during the late Cretaceous (Cai et al., 2012). Thus the sandstones in the mélange at Sangsang and Ngamring are interpreted to be derived from Asia and incorporated into the subduction complex during oceanic subduction along the southern margin of Asia. Cai et al. (2012) identified a turbiditic unit, the upper member of the Rongmawa Formation, which is fault-bounded in the mélange, yielded detrital zircon ages similar to those from the sandstone blocks, and was interpreted as Asian-derived trench fill (Cai et al., 2012). About 30 km east of Lazi, ~300 km east of the Lopu Range (Fig. 1), three groups of sandstone blocks have been identified (An et al., 2017). The first is interpreted to be derived from Tethyan Himalaya strata, the second to represent trench fill that bypassed the filled forearc basin at ~94 Ma, and the third to be syn-collisional foreland basin strata deposited at ~54 Ma (An et al., 2017). In the Renbu area, ~500 km east of the Lopu Range (Fig. 1), the siliclastic matrix mélange contains sandstone blocks with Paleozoic and older detrital zircon age populations as well as Mesozoic populations that share the same age peaks and lulls with the Gangdese magmatic arc and Xigaze forearc basin (Li et al., 2015b). Sandstone petrography on these blocks falls within the recycled orogen field, and Hf isotopic signatures are consistent with the juvenile Gangdese magmatic arc and those of more evolved igneous rocks and sediments in the central and northern Lhasa terrane.

The Zhongba-Gyangze Thrust (ZGT) places siliciclastic matrix mélange in the north on Tethyan Himalayan strata in the south (Burg and Chen, 1984; Ratschbacher et al., 1994; Ding et

al., 2005). The fault was originally south-verging and north-dipping (Burg and Chen, 1984; Ratschbacher et al., 1994; Ding et al., 2005), but in some locations it has been modified so that it now dips to the south (Wang et al., 2017). The Tethyan Himalaya strata were deposited on the northern passive margin of India during Paleozoic-Paleocene time. They are bounded to the north by the YSZ and to the south by the north-dipping South Tibetan Detachment System, which exposes high-grade rocks of the Greater Himalayan Sequence in its footwall (Fig. 1). From south to north the units deepen from platform deposits to carbonaceous flysch and turbidites (Liu and Einsele, 1994). The Lower Permian and Lower Triassic strata were deposited in rift settings, whereas Jurassic to Paleocene strata were part of the passive margin sequence (Garzanti, 1999). Lower Cretaceous volcaniclastic rocks, including the Wölong Formation, are locally interbedded with 145 to 115 Ma intra-plate volcanic rocks (Hu et al., 2015c and references therein). Early Cretaceous zircon peak ages vary in Tethyan strata. Those in the Northern Tethyan Himalaya are similar to the Comei igneous province (~132 Ma), those in the Lesser Himalaya strata are similar to the Rajmahal-Silhet igneous province (~117 Ma), and those in the southern Tethyan Himalaya fall in between (Hu et al., 2015c). The Comei and Rajmahal-Silhet igneous provinces developed in northeastern India during the breakup of India and Australia, and river systems distributed volcanic clasts along the northern margin of Greater India from east to west (Hu et al., 2015c and references therein).

The Cretaceous – Paleocene Sangdanlin section ~8 km south of Saga (Fig. 1) records the transition from Indian- to arc-derived detritus at 60-58.5 Ma, marking the initiation of India-arc collision (Ding et al., 2005; Wang et al., 2011; DeCelles et al., 2014; Wu et al., 2014; Hu et al., 2015a). Interpretations of the structural setting of the section range from fault-bounded in the mélange (Wang et al., 2011) to fault-bounded by Tethyan Himalaya strata (Yang et al., 2003) to

conformable on Cretaceous Tethyan Himalaya strata to the south and in a footwall syncline to the north where siliciclastic matrix mélange is thrust southward (Ding et al., 2005; DeCelles et al., 2014). The three formations of the Sangdanlin section are conformable and in depositional contact with one another (Ding et al., 2005; Wang et al., 2011; DeCelles et al., 2014).

The lowermost formation of the Sangdanlin section, the Upper Cretaceous to Danian (Hu et al., 2015a) Denggang/Zhongzuo Formation (~100 m thick), coarsens upward and is dominated by red and green siliceous shale and siltstone in the lower part and massive quartzose sandstone in the upper part. Shale and siltstone layers are interbedded with chert, fine-grained green lithic sandstone, and medium-grained to pebbly quartzarenite sandstone (Ding et al., 2005; Wang et al., 2011; DeCelles et al., 2014). The base of the Upper Danian to Lower Selandian (Hu et al., 2015a) Sangdanlin Formation (~100 m thick) is a sharp contact between coarse-grained quartzose sandstones in the upper part of the Denggang/Zhongzuo Formation and red and green shale, chert, and porcelanite. Some feldspatholithic sandstone beds occur in the middle part of the Sangdanlin Formation, and its upper part is dominated by red siliceous shale (Wang et al., 2011; DeCelles et al., 2014). The boundary between the Sangdanlin Formation and the overlying late Selandian (Hu et al., 2015a) Zheya Formation (~500 m) is marked by the transition from red and green colored to gray colored shale, chert, and porcelanite. The Zheya Formation overall coarsens upward and contains thickening and coarsening upward sequences of feldspatholithic sandstone beds. Chert beds are present in the lower part of the formation, and conglomerates, along with olistostromal blocks, are present in the upper parts of the published sections (Ding et al., 2005; Wang et al., 2011; DeCelles et al., 2014).

Provenance changes in the Sangdanlin section are observed in both sandstone petrography and in detrital zircon age populations. Sandstone layers from the Denggang/Zhongzuo Formation

311 are composed almost entirely of quartz (Wang et al., 2011; DeCelles et al., 2014) and consist of
312 two detrital zircon signatures: one signature with no grains younger than ~490 Ma (DeCelles et
313 al., 2014; Wu et al., 2014) and one signature that is similar to the first but includes a prominent
314 early Cretaceous age population, coeval with the Tethyan Wölong volcaniclastic rocks (Wang et
315 al., 2011; Hu et al., 2015a). In the Sangdanlin Formation, sandstones alternate between quartz-rich
316 sandstones yielding >490 Ma zircon age populations, quartz-rich to lithic sandstones of Wölong
317 affinity, and lithic sandstones with late Cretaceous and Paleocene age populations and lesser pre-
318 Mesozoic populations (Ding et al., 2005; Wang et al., 2011; DeCelles et al., 2014; Wu et al., 2014;
319 Hu et al., 2015a). The Zheya Formation is dominated by lithic sandstones with late Cretaceous and
320 Paleocene age populations and lesser pre-Mesozoic populations (Ding et al., 2005; Wang et al.,
321 2011; DeCelles et al., 2014; Wu et al., 2014; Hu et al., 2015a). DeCelles et al. (2014) dated a
322 tuffaceous layer ~450 m above the base of the Zheya Formation at 58.5 ± 0.6 Ma. Ophiolitic
323 material in the form of serpentinite clasts and high-Cr, low-Ti spinels has been observed in the
324 Sangdanlin Formation (Ding et al., 2005; Aitchison et al., 2007; Wang et al., 2011; Wu et al., 2014;
325 Baxter et al., 2016) and the Zheya Formation (Wang et al., 2011) and used as evidence of
326 Paleocene India-intraoceanic arc collision (Aitchison et al., 2007; Baxter et al., 2016) or India-
327 Asia collision (Ding et al., 2005; Wang et al., 2011; Wu et al., 2014). Based on the age and
328 provenance patterns in the Sangdanlin section, the change from Indian provenance to arc
329 provenance occurred during deposition of the Sangdanlin Formation at ~59 Ma (DeCelles et al.,
330 2014; Hu et al., 2015a).

331 Other arc-affinity Paleocene foreland basin deposits are documented at Gyangze (Cai et
332 al., 2011; Wu et al., 2014), south of Sangsang (Wang et al., 2017), and ~30 km east of Lazi (An et
333 al., 2017)(Fig. 1). Eocene foreland basin deposits are documented farther south in the Zhepure

Mountain region near Tingri (Willems et al., 1996; Zhu et al., 2005; Najman et al., 2010; Hu et al., 2012), near Gamba (Willems and Zhang, 1993; Zhang et al., 2012; Li et al., 2015c), and near Mt Kailas (~300 km northwest of Zhongba, the Dajin Formation) (Wang et al., 2015). Studies near Gamba and Tingri also document stratigraphic changes during the Middle Maastrichtian to Paleocene that are consistent with flexural responses due to the initiation of collision farther north (Willems et al., 1996; Zhang et al., 2012; Li et al., 2015c).

3. Geology of the study area: the Lopu Range

We conducted geologic mapping and sampling in the Lopu Range (Fig. 2) ~50 km northwest of Saga (Fig. 1). The Xigaze forearc, geology of the Lopu Range, adjacent siliciclastic matrix mélange, and imbricated Tethyan Himalaya strata were all investigated simultaneously. The focus of this paper is the siliciclastic matrix mélange and the structurally imbricated Tethyan Himalaya strata to the south. We refer to Orme et al. (2015), Laskowski et al. (2016), and Laskowski et al. (2017) for details of the geology of the forearc basin and core of the Lopu Range.

Northeast of the Lopu Range, The Kailas Formation is deposited on the Gangdese magmatic arc, and the Xigaze forearc basin strata are thrust northeast over the Kailas Formation along the northernmost strand of the GCT (Fig. 2). A strand of the GCT thrusts the siliciclastic matrix mélange northeast over forearc basin strata in the footwall. Ophiolitic mélange is locally exposed in the hanging wall of the GCT thrust over the forearc basin strata, and the YZMT places the ophiolitic mélange over the siliciclastic matrix mélange to the southwest (Fig. 2). The siliciclastic matrix mélange is exposed structurally above meta-Tethyan Himalaya strata in the core of the Niuku anticline on both the northern and southern sides of the Lopu Range, in the hanging wall of the originally south-directed ZGT, which has since been folded (Ding et al., 2005; Laskowski et al., 2016; Laskowski et al., 2017). On the south side of the Lopu Range, the ZGT

dips southwest beneath the siliciclastic matrix mélange and is exposed again farther south dipping to the northeast (Fig. 2). Hence, the siliciclastic matrix mélange is everywhere fault bounded. Imbricated Tethyan Himalaya strata are in the footwall of the ZGT to the south (Fig. 2).

4. Composition and Structure of the Subduction Complex

To determine the composition, provenance, structural architecture, and extent of the YSZ subduction complex, we mapped siliciclastic matrix mélange and imbricated Tethyan Himalaya strata around the Lopu Range at a scale of 1:100,000. Geologic mapping and sampling were conducted during traverses on foot. We present our new stratigraphic and structural data in Figure 2.

4.1. Siliciclastic matrix mélange

The siliciclastic matrix mélange is characterized by a block-in-matrix structure with decimeter to m×km blocks in a shale matrix with occasional sandstone (Fig. 3a). No imbricated sections of ocean plate stratigraphy were observed within the siliclastic matrix mélange, consistent with previous studies. The blocks consist of shale, chert, metabasite, basalt, limestone, sandstone, and phyllitic shale (Figs. 3b,c,d). Chert and limestone blocks are most abundant, basalt and metabasite blocks are less common, and sandstone and shale blocks are rare and only locally exposed in the siliciclastic matrix mélange. Every sandstone block found during traverses in the mélange was sampled and analyzed for U-Pb detrital zircon geochronology and sandstone

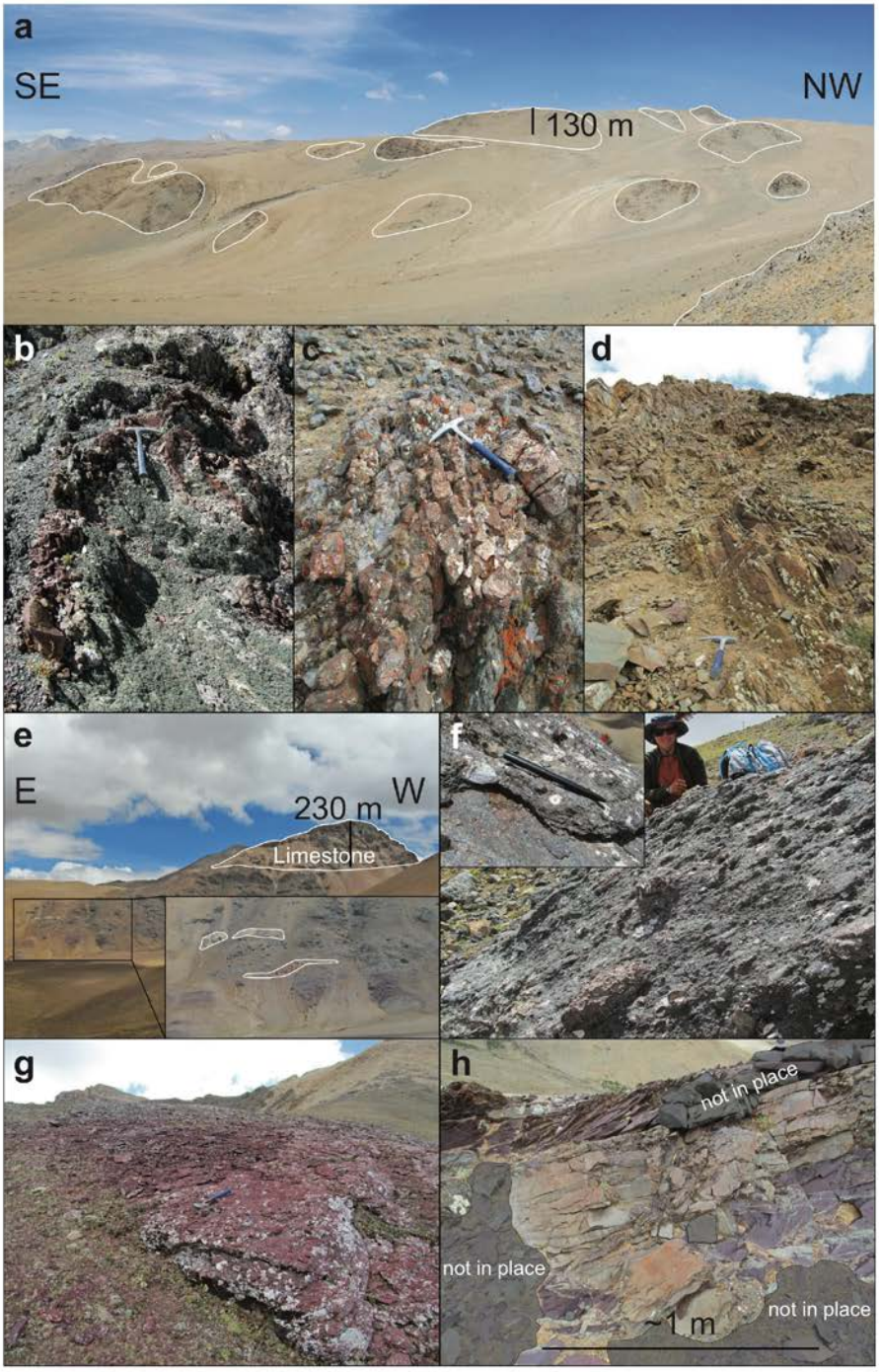
a
SE
NW
130 m
b
c
d
e
E
230 m
W
Limestone
f
g
h
not in place
not in place
not in place
~1 m

Figure 3

375

Figure 3. Siliciclastic matrix mélange field photos. (a) Block-in-matrix structure. Blocks are the more resistant exposures (outlined in white), and the more recessive matrix underlies the hillslopes. (b) Transposed green and red shale. (c) Greenschist-facies pillow basalt block. (d) Sandstone block with primary bedding preserved. (e) Large limestone block (outlined in white) caps the mountain and purple-blue-green shale matrix forms the lower slope beneath the block. The inset shows smaller sigmoidal limestone blocks. (f) The only conglomerate observed in the block-in-matrix mélange. The inset shows a crinoid stem in green and purple shale. (g) Basalt block showing a pervasive red color. (h) An outcrop of the matrix between the blocks is composed of cleaved purple shale and highly deformed green sandstone. Shaded areas are talus or Mani stones.

petrography (Fig. 2). Locally exposed pillow basalts exhibit shear fabrics between pillows, and the vesicles are filled with sheet silicate minerals and calcite (Fig. 3c). Chert blocks locally exhibit pencil cleavage. The largest blocks are limestone which are in most places 10s of meters in stratigraphic thickness, but can be kilometers long and are massively bedded with occasional concentrations of crinoid stems and other fossils (Fig. 3e). One block of conglomerate was observed in the block-in-matrix mélange; it includes boulders to cobbles composed of reworked matrix shale with occasional crinoid ossicles and coral fragments, green and purple metabasite, fine-grained purple sandstone, and green and purple shale (Fig. 3f). This conglomerate likely formed by slope failure and mass wasting from the subduction complex. Individual sedimentary blocks locally preserve primary depositional contacts (Fig. 3d). The minerals in mafic and calcareous blocks are in many places altered to a red, purple, or green color (Fig. 3g). The matrix is composed of transposed and cleaved red, purple, and green shale with occasional fine-grained sandstone (Fig. 3h). Sandstone-bearing matrix tends to be better exposed than mostly recessive shale-only matrix. Where observed, the matrix exhibits both soft-sediment deformation and tectonic deformation such as pervasive cleavage at an angle to bedding planes (Fig. 3h).

Fabrics within the blocks include bedding, cleavage, veins, foliation, and lineation, and some blocks are more deformed than the mélange matrix. Fabric orientations within the blocks and matrix, however, are highly variable (Fig. 2). Due to the large size of blocks and the generally poor exposure of the siliciclastic matrix in the study area (Fig. 3a), detailed observations of block shape, matrix fabric, and relationships between matrix deformation and block deformation were difficult to ascertain. However, a rare cliff exposure (Fig. 3e) shows sigmoidal limestone phacoids with similar orientations to the surrounding matrix, indicative of a tectonic mélange. Given that the composition of blocks is consistent with dismembered ocean plate stratigraphy, the blocks are

variably deformed, and the matrix shows a mixture of sedimentary and tectonic deformation, it is likely that the siliclastic matrix mélange is composed of both tectonically deformed sedimentary mélanges and tectonic mélange. Sedimentary mélanges would have formed by slope failure into the trench, and subduction tectonism would have overprinted the sedimentary mélanges and formed new tectonic mélange as ocean plate stratigraphy was dismembered.

4.2. Imbricated Tethyan Strata

Over a distance of ~10 km to the southwest of the town of Lazangxiang (Fig. 2), siliciclastic blocks gradually increase in size and ultimately transition into ~2 km x ~10 km north-dipping thrust sheets of coherent, sandstone-rich sedimentary units, and the component of matrix gradually decreases (Fig. 4a,b). Intervals of deformed shale with minor sandstone are highly deformed between less deformed blocks of siliciclastic strata (Fig. 4a,b). We interpret the deformed shale intervals as mélange matrix rather than deformed bedding in the stratigraphic section because the purple and green shale is ubiquitous in the mélange but absent in Tethyan stratigraphy in this region or along-strike, and in places the deformed shale intervals cut across coherent stratigraphy. Southwest of this 10-km-wide transitional zone, the matrix is absent and deformation is localized along incompetent layers within coherent stratigraphic sections. Strain markers are also present in the competent layers in the form of small bedding-non-parallel slicken surfaces and minor meter-scale folding and faulting. Bedding generally dips north to northeast (Fig. 2, Fig. 4a). The coherent stratigraphy is mostly siliciclasitc, with sandstones ranging from coarse pebbly quartzarenite (Fig. 4c) to fine-grained volcaniclastic green sandstone (Fig. 4d). Sandstone is in many places interbedded with brown or black shale. Layers of laminated red, green, gray, and black chert are intercalated with shales of similar color. Minor

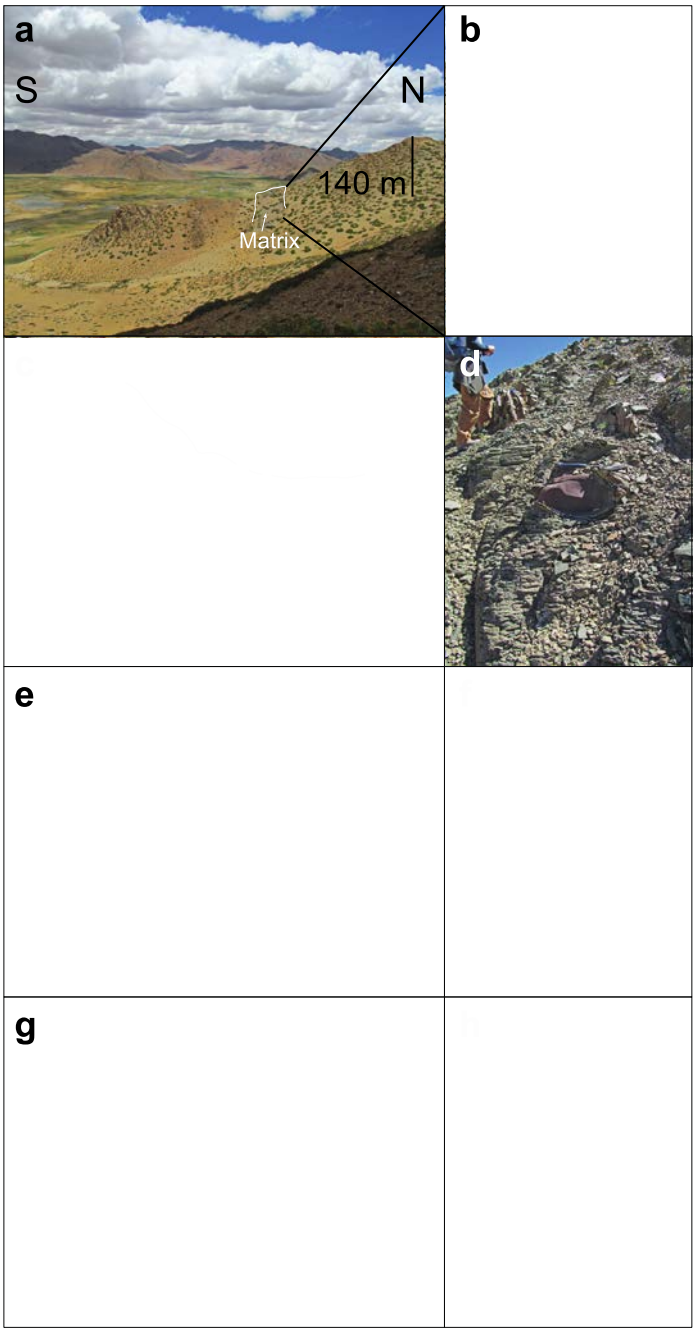

430

Figure 4. Imbricated Tethyan Himalaya strata field photos. (a) Thrust sheets of continuous stratigraphy separated by matrix. (b) Matrix separating the thrust sheets in a. The matrix is composed of purple shale and highly deformed green sandstone. Orientations vary widely. (c) Scour base in Tethyan Himalaya strata separating medium-grained quartzarenite below from pebbly quartzarenite above. (d) Rounded limestone olistolith in fine-grained green sandstone. (e) Cobble to boulder conglomerate with clasts of limestone and chert. (f) Variably recrystallized sandstone. The sandstone above and below the hammer is recrystallized and much more cohesive than the sandstone in the middle. (g) Brecciated sandstone with slicken surfaces. (h) Dismembered sandstone beds enveloped in less competent shale.

beds of crinoid-bearing limestone, laminated limestone, red-green laminated shale, dirty chert or porcelanite, metabasite, and cobble to boulder conglomerate with clasts of limestone and chert (Fig. 4e) are interbedded with the sandstone. Two m-scale olistoliths were observed: a limestone in green sandstone (Fig. 4d), and a purple sandstone in red chert and shale. The quartzarenite sandstones are variably recrystallized (Fig. 4f), and recrystallized sandstones are locally brecciated (Fig. 4g). Sections of interbedded sandstone and shale are locally dismembered (Fig. 4h).

5. Methods

5.1. U-Pb detrital zircon geochronology

We sampled sandstones across the mélange (*n = 15*) and imbricated Tethyan Himalaya strata (*n = 11*) to determine their provenance by U-Pb dating of detrital zircons. Zircons were recovered from samples using standard crushing and separation methods, mounted in epoxy, polished, imaged by back-scattered electrons (BSE) using a scanning electron microscope (SEM), and dated using a laser-ablation multicollector inductively-coupled plasma mass spectrometer at the Arizona LaserChron Center (methods described in Gehrels et al., 2008). All samples were analyzed using a 35 μm beam except for finer-grained zircons in sample 7.3.12.3KM which were analyzed with a 25 μm beam. We dated 3,002 grains, 753 of which were excluded because of discordance (>20%), reverse discordance (>10%), high common lead (>100 counts per second), or high error in ages (>10%). Most of the excluded grains had high common lead. Here we present 2,249 new detrital zircon U-Pb ages. Because of the paucity of post-Cambrian zircons in Tethyan Himalayan strata, the maximum depositional age determined by zircon populations does not approximate the depositional age of Tethyan Himalayan strata, so we do not calculate maximum depositional ages for these samples. The youngest population of zircon ages in arc-derived sandstones may approximate their true depositional age (Dickinson and Gehrels, 2009; Painter et

al., 2014), hence we report maximum depositional ages for samples with arc detrital zircon signatures.

We explored several methods for determining the maximum depositional age (MDA) of each sample: 1) the peak age of the youngest zircon population (3 or more grains) within two-sigma uncertainty, which does not contain a magnitude of error; 2) the weighted mean age of the youngest zircon population (3 or more grains) within 2σ uncertainty, which provides an MSWD but requires a defined population; 3) the age provided by the isoplot tool TuffZirc which requires at least 10 analyses, removes analyses with anomalously high uncertainties, ranks the analyses by $^{206}Pb/^{238}U$ age, and takes the median of the largest cluster of ages with $p>0.05$ as the true age with asymmetric analytical uncertainties (Ludwig and Mundil, 2002); and 4) the unmixed age which uses the Sambridge-Compston algorithm to fit Gaussian curves to the data, allowing a determination of age uncertainties but requiring a choice of the number of peaks to calculate. We used a combination of methods 2 and 4 and prescreening. We first screened the youngest group of three or more ages that overlapped within 2σ uncertainty. Grains with anomalously high U concentration which might be affected by lead loss and those with anomalously high U/Th ratios which might be affected by fluids post-crystallization were excluded in each case. We then used the unmixing algorithm to determine the youngest population of grains. Finally, we calculated the weighted mean age of that population to examine the MSWD of that population. MSWD values ≤ 1 indicate that the age uncertainty is sufficient to explain the scatter in ages and gives us confidence that the grains are cogenetic, while MSWD values >1 indicate that the age uncertainty is insufficient to explain the scatter and that the grains may not be cogenetic.

5.3. Sandstone and metamorphic petrography

We prepared thin sections for sandstone petrography from 22 of the 26 sandstone samples analyzed for detrital zircon dating. The thin sections were stained for K-feldspar and Ca-plagioclase. We counted 450 grains for each sample using the Gazzi-Dickinson method (Gazzi, 1966; Dickinson, 1970; Ingersoll et al., 1984). We analyzed petrographic thin sections of three metabasite and four metapelite blocks from the siliciclastic matrix mélange cut perpendicular to foliation and parallel to lineation. For each sample, we identified minerals and textures with a petrographic microscope and acquired mineral chemistry with electron microprobe analyses. The uncovered thin sections were coated with carbon and analyzed with a CAMECA SX100 Ultra using an accelerating voltage of 15 keV, a beam current of 2-20 nA, a beam diameter of 5 μm, and a counting time of 10-20s. Both titanite and apatite grains lacked sufficient uranium for U-Pb geochronology.

6. Results

6.1. U-Pb detrital zircon geochronology and sandstone petrography

Full results of detrital zircon analyses are included in the supplementary data. Recalculated modal compositions for sandstone petrography are in Table 1. We identified three groups of samples based on the youngest detrital zircon age populations present in each sample (Fig. 5). The first group is characterized by age spectra with no populations of grains <~400 Ma. Zircon ages ranging from 450-650 Ma exhibit a major age peak at 500-520 Ma. Additional peaks are at 800-1200 Ma and 2400-2500 Ma. Sandstone petrography places almost all of the samples in the first group in the continental interior field with 80% or more quartz (Fig. 6). Matrix sandstone sample 7.3.12.3KM falls in the recycled orogenic field and contains some early Cretaceous grains, though not enough to comprise a significant population. Lithic grain compositions vary widely and make up <15% of the grains counted. The second group of

508 Table 1. Recalculated petrographic data

Sample	Qm%	F%	Lt%	Qt%	F%	L%	Qm%	P%	K%	Lm%	Lv%	Ls%
6.19.12.3KM	85.1	0.2	14.6	85.6	0.2	14.2	99.7	0.3	0.0	29.7	67.2	3.1
6.19.12.8KM	99.3	0.0	0.7	99.3	0.0	0.7	100.0	0.0	0.0	0.0	0.0	0.0
6.19.12.9KM	82.6	7.5	9.9	84.2	7.1	8.7	91.7	8.3	0.0	9.5	28.6	61.9
6.21.12.2KM	99.8	0.0	0.2	99.8	0.0	0.2	100.0	0.0	0.0	100.0	0.0	0.0
7.3.12.3KM	47.2	9.8	43.0	52.5	8.9	38.6	82.8	17.2	0.0	2.9	95.4	1.7
6.27.12.4KM	99.8	0.0	0.2	99.8	0.0	0.2	100.0	0.0	0.0	0.0	0.0	100.0
6.22.12.7KM	98.8	0.0	1.2	98.9	0.0	1.1	100.0	0.0	0.0	0.0	80.0	20.0
6.22.12.1KM	92.5	0.0	7.5	92.9	0.0	7.1	100.0	0.0	0.0	0.0	12.5	87.5
6.28.12.5KM	88.0	5.6	6.3	88.5	5.4	6.1	94.0	5.0	1.0	3.6	67.9	28.6
6.29.12.4KM	92.4	5.7	1.9	92.9	5.4	1.8	94.2	5.8	0.0	22.2	33.3	44.4
6.19.12.2KM	50.2	15.6	34.1	53.6	14.6	31.8	76.3	23.7	0.0	6.3	92.3	1.4
6.19.12.4KM	90.6	4.0	5.4	91.3	3.8	4.9	95.8	4.2	0.0	13.0	69.6	17.4
6.19.12.6KM	61.1	12.9	26.0	62.9	12.4	24.7	82.6	17.4	0.0	1.8	91.2	7.0
6.19.12.7KM	77.8	3.9	18.3	78.9	3.8	17.3	95.2	4.8	0.0	1.3	87.3	11.4
7.3.12.4KM	100.0	0.0	0.0	100.0	0.0	0.0	100.0	0.0	0.0	0.0	0.0	0.0
6.22.12.4KM	39.1	37.7	23.2	44.4	34.4	21.2	51.0	49.0	0.0	4.2	90.6	5.2
6.28.12.3KM	58.8	13.6	27.6	62.4	12.4	25.1	81.3	18.1	0.7	0.0	79.8	20.2
6.29.12.1KM	79.3	2.7	18.0	79.8	2.7	17.6	96.7	3.3	0.0	2.5	63.3	34.2
6.30.12.1KM	81.2	5.2	13.6	81.6	5.1	13.3	94.0	5.8	0.3	1.6	31.1	67.2
6.30.12.2KM	53.8	17.1	29.0	56.8	16.1	27.1	75.8	22.8	1.3	0.8	32.8	66.4
6.17.12.13KM	41.2	28.2	30.6	49.6	24.2	26.2	59.3	40.7	0.0	10.9	88.2	0.8
6.29.12.3KM	51.9	19.2	28.9	55.3	18.2	26.4	72.9	27.1	0.0	5.6	87.9	6.5

509

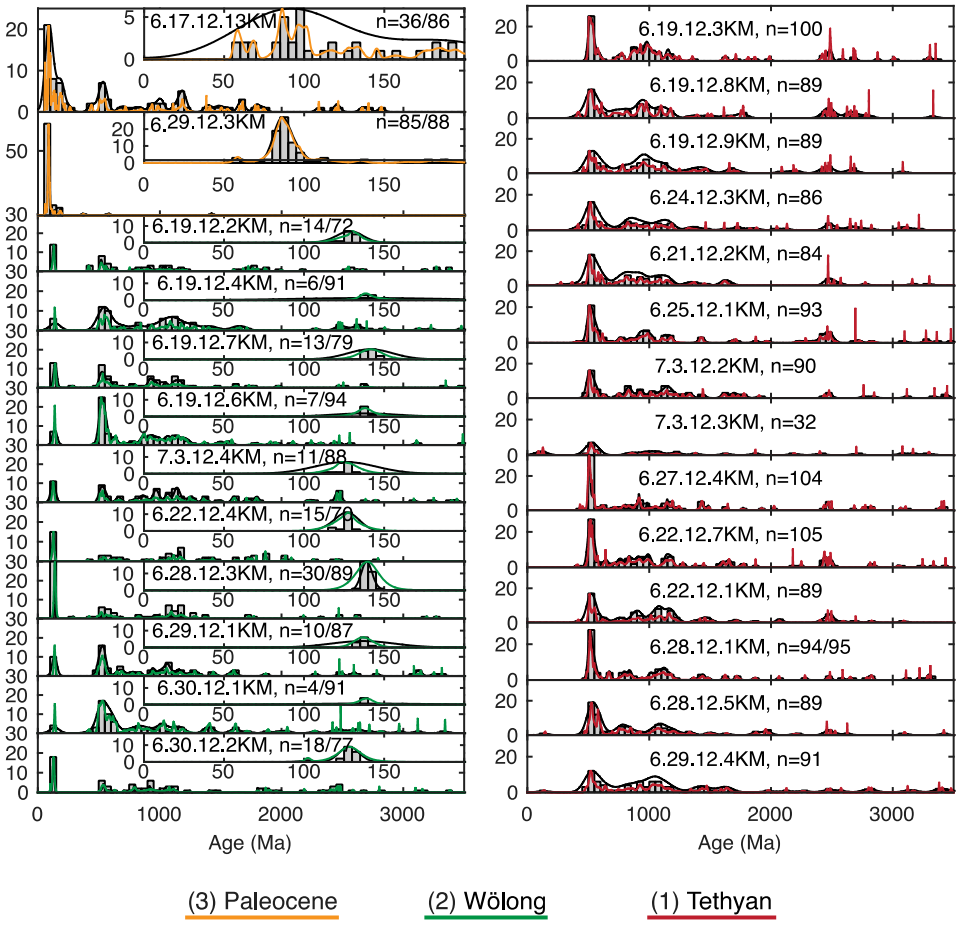

Figure 5

Figure 5. Detrital zircon U-Pb ages from sandstones in the siliciclastic matrix mélange and the imbricated Tethyan Himalaya strata in the Lopu Range region. Ages are shown as histograms, probability density functions in colored curves, and kernel density estimations in black curves; n is the number of grains in the format n=number in the subplot/number in the full plot/number in the sample if some grains are older than 3500 Ma. Only relevant numbers are reported. Inset plots show ages <200 Ma with 5 Ma histogram binwidth, and full plots show ages <3500 Ma with 50 Ma histogram binwidth. Note y-axis scale varies.

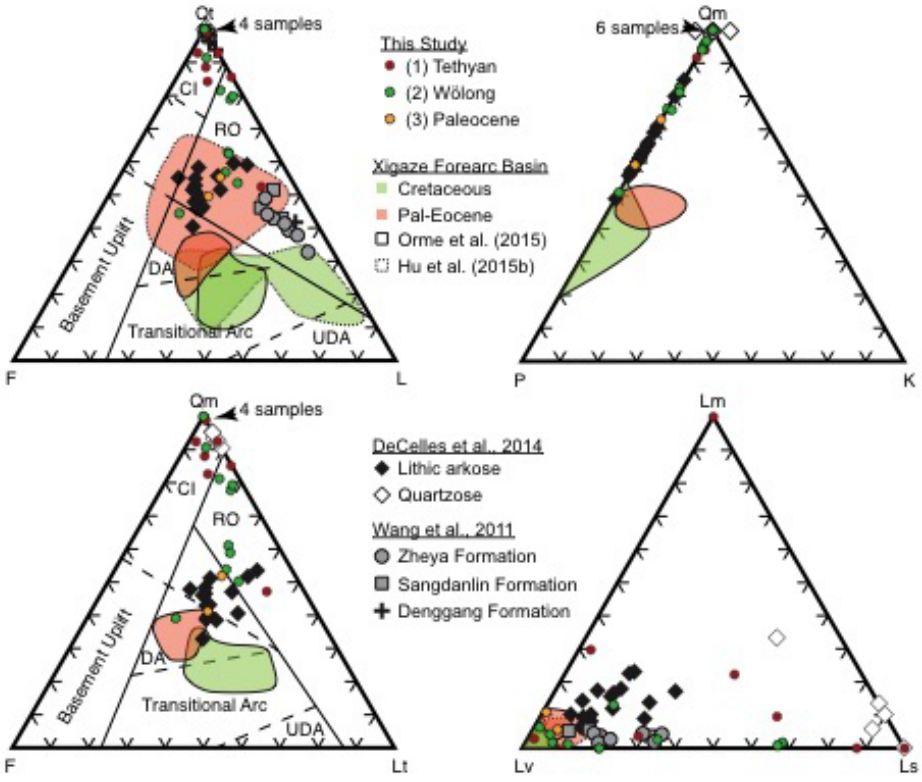

Figure 6

Figure 6. Sandstone petrography ternary plots and comparison with previous studies. Provenance fields after Dickinson et al. (1983). CI: continental interior, RO: recycled orogen, DA: dissected arc, UDA: undissected arc. Recalculated petrographic data are displayed in table 1.

samples is characterized by age spectra with the same peaks as the first group and an additional peak at 125-140 Ma with a gap in between (Fig. 5). Although they have the same detrital zircon populations, the sandstone petrography for the second group is divided between the recycled orogen and continental interior fields with 50% or more quartz (Fig. 6). Matrix sandstone sample 6.22.12.4KM falls into the dissected arc field with <50% quartz. Lithic grain compositions range from mostly igneous to nearly equal percentages of sedimentary and igneous lithic grains. The third group is characterized by age spectra with <400 Ma peak ages at ~180 Ma, ~85 Ma, and as young as 58.5 Ma and consists of only two samples: 6.17.12.13KM and 6.29.12.3KM (Fig. 5). Sample 6.17.12.13KM includes the same older peaks as the two previous groups, although they are not as prominent because ~42% of the grains are <200 Ma. The youngest age population overlapping in uncertainty consists of four grains with similar U concentrations and U/Th ratios. The weighted mean age of these four grains is 58.4±2.9 Ma, with MSWD of 1.2. Sample 6.29.12.3KM contains no older peaks as >95% of the grains are <200 Ma. Most of the grains in this sample overlap within uncertainty, but the unmixing algorithm identifies a clear peak at 58.8 Ma. The peak is composed of four grains with similar U concentrations and U/Th ratios. The wieghted mean age of these four grains is 58.5±2.3 Ma, with MSWD of 0.36, suggesting that the grains are cogenetic. Sandstone petrography places these two samples near the transition between the recycled orogenic and dissected arc fields (Fig. 6). Lithic compositions are >80% igneous. Samples from all three groups contain little to no K-feldspar (Fig. 6).

6.3. Metamorphic petrography

The metabasites have a mineral assemblage qtz+cal+chl+ms+Fe-oxide±ab±ttn±ap ±aln±ep±rt and the metapelites have a mineral assemblage qtz+cal+chl+ms+ab+Fe-oxide±rt±ttn±ap±aln±ep±bt±or (Table 2). Metabasite samples generally have a plagioclase lath

545 Table 2. Mineral assemblages of metamorphic samples. Samples are metapelites unless
546 otherwise specified.

Sample	6.16.12.3KM	6.17.12.15KM	6.19.12.11KM	6.20.12.1KM	6.17.12.3KM*	6.17.12.6KM*	6.17.12.7KM*
Albite	X	X	X	X	X	X	
Epidote	X				X		
Allanite	X	X			X		X
Chlorite	X	X	X	X	X	X	X
Calcite	X	X	X	X	X	X	X
Biotite				X			
Muscovite	X	X	X	X	X	X	X
Quartz	X	X	X	X	X	X	X
Sphene	X	X		X	X		X
Apatite		X		X		X	X
K-feldspar				X			
Iron Oxide	X	X	X				
Iron Oxide with Ti				X	X	X	X
Rutile with Fe					X		
Rutile - minor Ca,Si,Fe	X	X	X				

* = metabasite

547

matrix and amygdaloidal texture (Fig. 7a). The vesicles are filled by intergrowths of quartz, chlorite, and muscovite with occasional calcite (Fig. 7a). Wherever calcite is present, single crystals are often mm-scale (Fig. 7b) and are frequently in contact with smaller quartz crystals. Secondary chlorite is pervasive in all samples, often forming in pressure shadows (Fig. 7a). Sample 6.19.12.11KM contains chlorite with an anomalous blue color in cross-polarized light (Fig. 7c), indicative of high Fe content and supported by microprobe analyses (Supplemental data). Four samples contain allanite, and in two of those the allanite is found as veins in epidote crystals (Fig. 7d). In sample 6.16.12.3KM, titanite is abundant in the matrix and occasionally found as inclusions in euhedral iron oxide (Fig. 7e). In other samples, iron oxides are more diffuse (Fig. 7f). Amphibole and phengite are absent in all samples.

7. Sandstone provenance

To determine the provenance of the sandstones in the siliciclastic matrix mélange and Tethyan Himalaya strata, we compare them with the published detrital zircon age populations and sandstone petrography of different units (Fig. 6, 8). The first group with no detrital zircon populations <400 Ma is similar to the quartzarenite sandstones of the Denggang/Zhongzuo (Wu et al., 2014; Wang et al., 2017) and to the pre-Cretaceous Tethyan and upper Lesser Himalayan strata (Gehrels et al., 2011). The pre-Cretaceous Lhasa terrane looks similar but lacks the prominent 2400-2500 Ma peak age (Gehrels et al., 2011). Sandstone petrography places the first group in the continental interior field, consistent with the quartzarenite sandstones of the Sangdanlin section and a passive margin or continental interior setting. The second group includes an early Cretaceous detrital zircon age peak that is similar to the Cretaceous Wölong volcaniclastic rocks in the Tethyan Himalaya and upper Lesser Himalayan strata

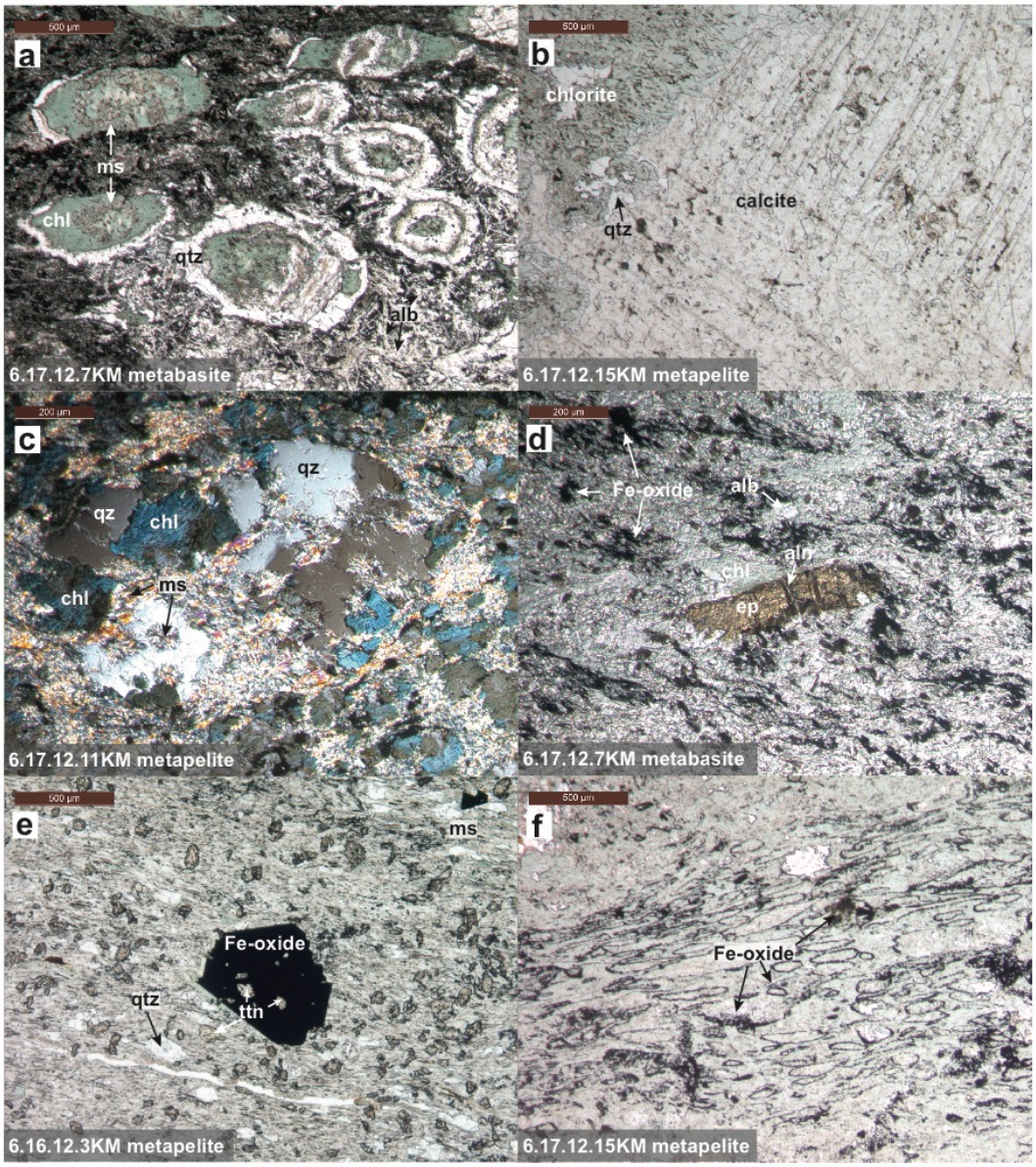
500 µm
a
ms
chl
qtz
alb
6.17.12.7KM metabasite
500 µm
b
chlorite
calcite
qtz
6.17.12.15KM metapelite
200 µm
c
qz
qz
chl
chl
ms
6.17.12.11KM metapelite
200 µm
d
Fe-oxide
alb
chl
ep
6.17.12.7KM metabasite
500 µm
e
ms
Fe-oxide
qtz
ttn
6.16.12.3KM metapelite
500 µm
f
Fe-oxide
6.17.12.15KM metapelite

Figure 7

571

572 Figure 7. Metamorphic petrology photomicrographs. All images are in plane-polarized light unless
573 specified. (a) Vesicles filled with intergrowths of quartz, chlorite, and muscovite. Chlorite forming
574 in pressure shadows. (b) Large calcite crystal. (c) Anomalous blue color in chlorite in cross-
575 polarized light. (d) Epidote crystal with allanite veins. (e) Titanite crystals in the matrix and within
576 iron oxide crystal. (f) Abundant iron oxide in the matrix. alb: albite, aln: allanite, chl: chlorite, ep:
577 epidote, ms: muscovite, qtz:quartz, ttn: titanite.

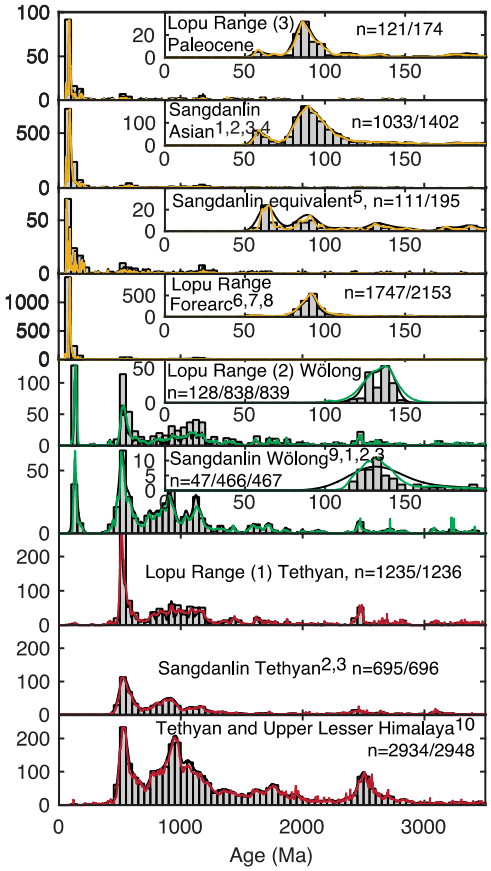

Figure 8

Figure 8. Comparison of detrital zircon ages of sandstones from the Lopu Range with detrital zircons from previous studies. Ages are shown as in figure 5. [1]Wang et al. (2011), [2]DeCelles et al. (2014), [3]Wu et al. (2014), [4]Hu et al. (2015a), [5]Wang et al. (2017), [6]Aitchison et al. (Aitchison et al., 2011), [7]Orme et al. (2015), [8]Hu et al. (2015b), [9]Hu et al. (2010), [10]Gehrels et al. (2011).

Figure 9. Tectonic model. (a) Forearc basin shoaling upward, and the accretionary wedge building on the southern margin of Asia by offscraping ocean plate stratigraphy from the Neotethyan slab. (b) Filling forearc basin and depositing Asian sediments on Tethyan Himalaya strata. (c) Incorporation of the Tethyan Himalaya strata into the siliciclastic matrix mélange as blocks and

thrust sheets, construction of the Tethyan thrust belt, and southward propagation of a flexural foreland basin system.

589 (Hu et al., 2010), and to the quartz-rich to lithic sandstones of the Sangdanlin Formation (DeCelles
590 et al., 2014; Wu et al., 2014; Hu et al., 2015a). Sandstone petrography places group 2 samples in
591 the continental interior and recycled orogenic fields with matrix sandstone sample 6.22.12.4KM
592 in the dissected arc field. Almost all of the sandstones sampled for detrital zircon analysis fall into
593 groups 1 or 2 and are of Tethyan affinity. Although matrix sandstone sample 7.3.12.3KM does not
594 have a significant early Cretaceous age population, there are early Cretaceous grains dated, and
595 the petrographic analysis is more consistent with the second group of samples. Therefore we
596 determine that sample 7.3.12.3KM is most likely of Cretaceous Wölong affinity.

597 The two samples in the third group contain mostly Mesozoic zircon ages, but >50% of the
598 zircons from sample 6.17.12.3KM are >200 Ma (Fig. 8). Sample 6.17.12.13KM is a schistose
599 arkosic sandstone block found in the mélange on the north side of the Lopu Range, and sample
600 6.29.12.3KM is an arkosic sandstone from the imbricated Tethyan Himalaya strata (Fig. 2). Both
601 samples have overlapping maximum depositional ages of 58.5 Ma and fall into the transitional
602 zone between dissected arc and recycled orogen (Fig. 6). With the exception of the early
603 Cretaceous Wölong volcaniclastic rocks, Mesozoic and Paleocene detrital zircon populations are
604 not derived from the Indian continent (Fig. 8), so these populations in group 3 must be derived
605 from an arc. The Paleocene sandstones in group 3 display the same peaks and lulls in the detrital
606 zircon age spectra and the same sandstone petrographic signature as the proximal Sangdanlin and
607 Zheya Formations (Wang et al., 2011; DeCelles et al., 2014; Wu et al., 2014; Hu et al., 2015a)
608 (Fig. 6, 8). We interpret the Paleocene sandstones of group 3 to be equivalent to those found in the
609 Sangdanlin and Zheya Formations.

610 The sandstone blocks in the mélange are indistinguishable from the imbricated Tethyan
611 Himalaya strata exposed in the south of the study area, and all sandstones analyzed in the study

612 area have detrital zircon and sandstone petrographic signatures similar to the formations of the
613 Sangdanlin section (Fig. 5, 6, 8). Although there are no measured sections in the imbricated
614 Tethyan Himalaya strata near the Lopu Range, the facies are similar to those found in the
615 Sangdanlin section. We interpret groups 1, 2, and 3 from the imbricated Tethyan Himalaya strata
616 south of the Lopu Range and from the sandstone blocks in the siliciclastic matrix mélange as
617 equivalent to the Sangdanlin section.

618 The arc-affinity sandstones in the siliciclastic mélange and the Sangdanlin section may
619 have been derived from either the Gangdese arc or an intraoceanic arc. However, the presence of
620 pre-Mesozoic detrital zircon populations in the mélange block, Sangdanlin Formation, and Zheya
621 Formation, is inconsistent with a Mesozoic – Paleocene intraoceanic arc. Older grains must have
622 been derived from a continental source. While there is evidence of interfingering between Indian-
623 affinity and arc-affinity detritus in the Sangdanlin section (DeCelles et al., 2014; Hu et al., 2015a),
624 there are clear similarities in U-Pb detrital zircon age and sandstone petrography between the
625 Paleocene Tethyan strata and the Xigaze forearc basin (Orme et al., 2015; Hu et al., 2015b). They
626 display the same peaks and lulls in the detrital zircon age spectra (Fig. 8), and the forearc basin
627 transitions from marine to fluvio-deltaic at ~59 Ma when fluvial systems could transport detritus
628 from the Xigaze forearc basin and its source region to the trench (Orme et al., 2015). Since the
629 Gangdese arc and the Lhasa terrane are sources of the Xigaze forearc basin (Dürr, 1996; Wu et al.,
630 2010; Aitchison et al., 2011; An et al., 2014; Dai et al., 2015; Orme et al., 2015; Hu et al., 2015b;
631 Orme and Laskowski, 2016), we interpret that the detrital zircon populations in the subduction
632 complex and Tethyan strata are Asian-affinity, derived from the Xigaze forearc basin, the
633 Gangdese arc, and the Lhasa terrane. The Paleocene arc-affinity sandstones are more
634 compositionally mature than the Paleocene Xigaze forearc basin sandstones northeast of the Lopu

Range (Orme et al., 2015), but overlap well with those northwest of the range (Hu et al., 2015b)(Fig. 6). Since the nearby Gangdese magmatic arc was active well into the Eocene, the maximum depositional age determined by detrital zircon ages is likely a good approximation of the true depositional age for these particular sandstones.

8. Metamorphism

The mineral assemblages found in metabasite and metapelite blocks from the siliciclastic matrix mélange are consistent with lower greenschist facies metamorphism. The lack of any relict cores of higher-facies phases could indicate that the samples were never at higher facies, although metasomatism, evidenced by the abundance of quartz and calcite, could have completely retrograded earlier higher grade mineral assemblages. Since both metabasite and metapelite blocks are metamorphosed to the same facies, it is unlikely that the metamorphism was related to metasomatism at spreading ridges or seamounts. The timing of metamorphism is poorly constrained, but likely occurred during subduction and/or continental collision. Based on their mineral assemblages and the lack of relict high-grade phases, it is likely that the blocks exposed in the mélange were not deeply subducted.

9. Discussion

9.1. Structure and composition of the siliciclastic matrix mélange

The siliciclastic matrix mélange contains blocks of mostly ocean plate stratigraphy with minor blocks of strata equivalent to the Sangdanlin section which are interpreted to have entered the trench during the final phase of mélange formation. The prevalence of ocean plate stratigraphy blocks (shale, chert, metabasite, basalt, and limestone) and dearth of terrigenous blocks supports the interpretation of the siliciclastic mélange as a subduction complex (Shackleton, 1981; Tapponnier et al., 1981; Searle et al., 1987; Cai et al., 2012) rather than deformed passive margin

658 strata (Aitchison et al., 2000). Structures in the siliciclastic mélange suggest that it is composed of
659 both tectonically deformed sedimentary mélange and tectonic mélange, consistent with a
660 subduction zone setting. The lack of any imbricated, coherent sections of ocean plate stratigraphy,
661 and dearth of trench fill strata in the siliciclastic matrix mélange, is anomalous when compared to
662 the type subduction complexes in the Franciscan and Japan. Rapid convergence between India and
663 Asia may have limited the thickness of ocean plate stratigraphy that was able to accumulate before
664 subduction (Clift and Vannucchi, 2004), promoting mélange deformation rather than imbricate
665 stacking.

666 The detrital zircon age spectra and sandstone petrography of the Paleocene sandstones in
667 the siliciclastic matrix mélange and Tethyan Himalaya show the same patterns as the Paleocene
668 forearc strata derived from the Gangdese arc and Lhasa terrane (Fig. 8), and we interpret the arc-
669 affinity sandstones to be of Asian affinity. The schistose deformation in the Paleocene sandstone
670 block in the siliciclastic matrix mélange, absent in any of the Tethyan strata observed in this area,
671 indicates that it was tectonically deformed in the mélange rather than deposited on the mélange
672 after the subduction complex became inactive, and we interpret that the other Tethyan blocks were
673 similarly incorporated into the mélange. As DeCelles et al. (2014) discussed, the Sangdanlin
674 section stratigraphy was deposited proximal to the continental margin of northern India, so
675 continental crust must have entered the trench by ~59 Ma. Therefore, the subduction zone south
676 of the ophiolite belt was active at the onset of India-Asia collision. Since the Paleocene sandstone
677 block from the mélange and the Paleocene sandstone bed from the imbricated Tethyan Himalaya
678 strata have the same maximum depositional age of 58.5 Ma, we suggest that it is unlikely that the
679 Tethyan sandstone blocks were incorporated before continental collision by mass wasting into the

trench, although there is a possibility that collision could have initiated earlier than 59 Ma if there was no sediment pathway from the forearc basin to the trench.

There is a clear transition from block-in-matrix deformation in the northeastern part of the study area, to imbricated blocks of Tethyan stratigraphy separated by matrix, to imbricated Tethyan stratigraphy to the southwest. This is the first documented exposure of deformation transitioning from oceanic subduction to the building of the Tethyan thrust belt as most other contacts along strike have been structurally buried by the GCT. It is likely that the Sangdanlin section near Saga is part of this zone of structural transition where a large block of Tethyan strata is surrounded by siliciclastic matrix mélange (Wang et al., 2011). The structural transition may be the result of increasing sediment thickness as the Indian margin entered the trench. Thinner, more distal strata may have been more easily broken into blocks, whereas thicker, more proximal strata may have deformed more readily as thrust sheets. Within the siliciclastic matrix mélange, Sangdanlin-equivalent blocks are exposed interspersed with blocks of ocean plate stratigraphy and very close to the forearc basin (Fig. 2). The complex structural history of the Lopu Range makes it difficult to determine if the distribution of blocks has been substantially altered since collision by folding and faulting during the development of the Lopu Range and the GCT. Structural doming of the siliciclastic matrix mélange in the Lopu Range may expose mélange emplaced near the Paleocene subduction interface which was more likely to contain the youngest accreted blocks. GCT overprinting is more prevalent to the north of the Lopu Range since the imbricated Tethyan strata generally retain their expected northward dip along south-verging thrusts (Fig. 2, Fig. 4a), but later faulting in a block-in-matrix mélange would be difficult to identify. None of the blocks exposed in the mélange record metamorphic conditions greater than lower greenschist facies,

although the Tethyan strata in the core of the Lopu Range underwent high pressure metamorphism (Laskowski et al., 2016).

Blocks of Cretaceous, Asian affinity sandstone documented along-strike (Cai et al., 2012; Li et al., 2015b; An et al., 2017; Wang et al., 2017) are notably absent in the Lopu Range area. While it is possible that our sample size is too small to rule out the presence of Cretaceous, Asian sandstone blocks in the siliciclastic matrix mélange, nearly all sandstone blocks and matrix in the mélange dated by detrital zircon geochronology are Mesozoic Asian-affinity (Cai et al., 2012; Li et al., 2015b; An et al., 2017; Wang et al., 2017), significantly different from our results. It is structurally problematic to accrete only the lower ocean plate stratigraphy without the overlying trench fill, so any Asian-derived trench fill that was present would have been incorporated and should be observable in the siliciclastic matrix mélange despite any additional deformation. In our study area, the Sangdanlin-equivalent Paleocene sandstone block was the only documented sand-sized trench fill from Asia that was accreted prior to or soon after Tethyan Himalaya strata entered the trench. Along strike near Ngamring (Fig. 1), Asian-affinity sandstones with MDA 200-85 Ma (using the method described in 5.1) were incorporated into the mélange, and Asian-derived trench fill with MDA 200-90 Ma was deposited on top of the mélange (Cai et al., 2012). These along-strike differences in provenance of siliciclastic matrix mélange sandstone blocks were likely controlled by the extent of forearc basin filling and sediment pathways to the trench (Cai et al., 2012). Although there was a Cretaceous sediment pathway from the forearc basin to the trench to the east of our study area, that sand-sized sediment was not transported along strike to the west as far as the Lopu Range region. This suggests that there was little or no axial transport in the trench or that sediment transport near Sangsang-Xigaze was directed west to east.

An un-breached outer forearc high in the Lopu region throughout the Cretaceous could have isolated the underfilled forearc basin from the trench, but what could have formed and maintained such a high is unclear. If the ophiolite acted as a high in this region, we would expect some ophiolitic material to be present in the forearc basin, but the forearc sandstones contain only minor serpentine (Orme et al., 2015). However, ophiolitic material in the Sangdanlin section suggests that the ophiolite was exposed at the time of collision. Subduction of a seamount chain could explain a persistent high in the forearc and in the trench, and basal subduction erosion could enhance forearc subsidence locally such that it remained underfilled later than in areas along strike to the east, but there are not significantly more limestone blocks derived from seamounts exposed in the mélange than elsewhere along strike or any other preserved record of a persistent seamount chain in the Lopu Range region. Another possible explanation for the lack of Cretaceous sandstones exposed in the mélange could be frontal subduction erosion of any trench fill and part of the accretionary complex. This is difficult to determine because the mélange architecture may have been overprinted by later collision-related deformation, but the subduction erosion rate could not have greatly exceeded the sediment delivery rate since 1) the ophiolite and forearc basin are preserved rather than tectonically eroded, 2) there are no forearc basement blocks in the mélange, a sign of a frontal prism, and 3) the Gangdese magmatic arc did not migrate consistently inboard during the Cretaceous.

9.2. Tectonic model

The sedimentological ties between the sandstone blocks in the siliciclastic matrix mélange, the Paleocene Tethyan strata, and the Paleocene Xigaze forearc basin strata suggest suturing between the Tethyan Himalaya and the Xigaze forearc at ~59 Ma. Since the Xigaze forearc is sourced from the Gangdese arc and the Lhasa terrane, we interpret the Paleocene India-arc

747 collision records India-Asia collision. This correlation suggests that the ophiolite belt formed in
748 the forearc of the Gangdese continental arc margin during early Cretaceous time and became the
749 basement to the Xigaze forearc basin beginning at 130-113 Ma (Marcoux et al., 1982; Girardeau
750 et al., 1984; Wang et al., 2012; An et al., 2014; Huang et al., 2015; Orme and Laskowski, 2016).
751 Paleocene collision between India and Asia creates a mismatch between convergence estimates
752 (4,000-5,000 km since 60 Ma)(Molnar and Tapponnier, 1975; Patriat and Achache, 1984; Besse
753 and Courtillot, 1988; Patzelt et al., 1996; Molnar and Stock, 2009; Copley et al., 2010; van
754 Hinsbergen et al., 2011a; Gibbons et al., 2015) and Cenozoic shortening estimates in Asia (750-
755 1,010 km since 55-50 Ma)(van Hinsbergen et al., 2011b; Li et al., 2015d) and in the Himalaya
756 (>650 km)(DeCelles et al., 2002; Li et al., 2015d). The timing of suturing between the Tethyan
757 Himalaya and the Xigaze forearc may be reconciled by two models: 1) the Tethyan Himalaya
758 represent a microcontinent rifted from India forming the Greater India Basin which subsequently
759 closed (van Hinsbergen et al., 2012) or 2) more convergence was accommodated in the Himalaya
760 than previously recognized. No suture has been recognized within the Himalaya or elsewhere in
761 the India-Asia system, and the problem of convergence and shortening remains an open question.
762 Based on the data presented in this study, any proposed tectonic model must include suturing of
763 the Xigaze forearc basin and the Tethyan Himalaya at ~59 Ma.

764 The siliciclastic matrix mélange formed on the southern margin of Asia by accretion of
765 ocean plate stratigraphy as well as forearc-basin-derived sandstones in the late Cretaceous near
766 Renbu (Li et al., 2015b), Lazi (An et al., 2017), Ngamring (An et al., 2017), and Sangsang (Wang
767 et al., 2017). The Tethyan Himalaya strata were part of the northern passive margin of Greater
768 India. Lower Cretaceous volcaniclastic rocks were deposited along most of the northern margin of
769 India and reworked in Upper Cretaceous – Paleocene Tethyan Himalaya strata (Jadoul et al., 1998;

Hu et al., 2010; Du et al., 2015; Hu et al., 2015c). During the Cretaceous in the Lopu Range region, unlike regions along-strike to the east, the forearc basin was underfilled and separated from the trench by an outer forearc high (Fig. 9a). Despite little to no trench fill, the subduction complex was slightly accretionary, incorporating blocks of oceanic crust and sediments, and deforming by block-in-matrix mélange formation. Limestone and basalt blocks were offscraped from subducting seamounts and incorporated into the subduction complex.

Based on the detrital zircon ages and petrography of the sandstones within the mélange and imbricated Tethyan Himalaya strata (Fig. 5, 6, and 8), we suggest that the record of the first interaction between Indian and Asian detritus is preserved in the study area (Fig. 8). The forearc basin strata shoaled upwards during the late Paleocene to early Eocene (Orme et al., 2015; Hu et al., 2015b), and the first Asian detritus deposited on Tethyan Himalaya strata in the study area has a maximum depositional age of ~59 Ma (Ding et al., 2005; Wang et al., 2011; DeCelles et al., 2014; Wu et al., 2014; Hu et al., 2015a), suggesting that the forearc basin became overfilled or that the subduction complex was erosionally breached as Tethyan Himalaya strata entered the trench at ~59 Ma (Fig. 9b). The two Paleocene sandstones with this maximum depositional age were likely derived from the forearc basin itself or sediments transported more distally from fluvio-deltaic systems in the forearc basin to the trench (Fig. 8) and are found both in the siliciclastic matrix mélange and within the imbricated Tethyan Himalaya strata (Fig. 2). We interpret these samples as a record of earliest Tethyan Himalaya – Xigaze forearc interaction. As the Tethyan Himalaya strata first entered the subduction zone they were broken up into blocks and incorporated into the mélange. As collision continued and thicker Tethyan strata entered the trench, deformation transitioned in time and space as deformation propagated southward: block-

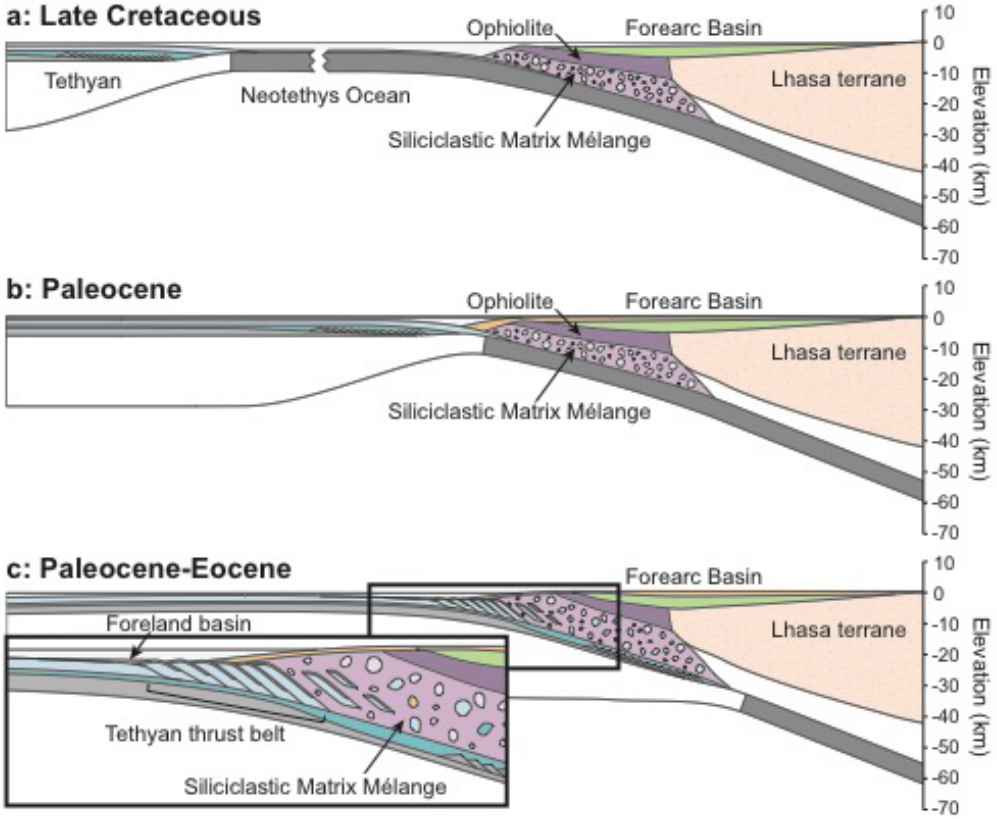

Figure 9

792

793 Figure 9. Tectonic model. (a) Forearc basin shoaling upward, and the accretionary wedge building
794 on the southern margin of Asia by offscraping ocean plate stratigraphy from the Neotethyan slab.
795 (b) Filling forearc basin and depositing Asian sediments on Tethyan Himalaya strata. (c)
796 Incorporation of the Tethyan Himalaya strata into the siliciclastic matrix mélange as blocks and
797 thrust sheets, construction of the Tethyan thrust belt, and southward propagation of a flexural
798 foreland basin system.

in-matrix mélange to the northeast, thrust sheets separated by matrix, and then imbricate thrusting in the southwest (Fig. 9c). Given the rapid convergence rate during Paleocene time (Molnar and Tapponnier, 1975; Patriat and Achache, 1984; Besse and Courtillot, 1988; Molnar and Stock, 2009; Copley et al., 2010; van Hinsbergen et al., 2011a; Gibbons et al., 2015) and the rapid southward propagation of foreland basin deposition (DeCelles et al., 2014), this transition in deformation likely occurred over a few million years at most.

10. Conclusions

The composition and structure of the siliclastic matrix mélange are consistent with a subduction complex formed by the accretion of ocean plate stratigraphy during Neotethyan subduction. Deformation exclusively by block-in-matrix formation may be a result of the rapid convergence between India and Asia and limited sediment pathways to the trench. Sandstones from the Yarlung Suture siliciclastic matrix mélange and Tethyan Himalaya strata in the Lopu Range region fall into three groups (Figs. 6 and 8). Group 1 samples have a Tethyan detrital zircon signtaure characterized by no age populations <~400 Ma and have >80% quartz, placeing them in the continental interior provenance field. Group 2 samples have a Wölong detrital zircon signature characterized by a Tethyan signature with an additional early Cretaceous peak age and have mixed sandstone petrographies in the continental interior or recycled orogen fields. Group 3 sandstones have a Xigaze forearc basin detrital zircon signature, a maximum depositional age of ~59 Ma, and sandstone petrography consistent with the Zheya Formation of the Sangdanlin section, more compositionally mature than the forearc basin strata. Therefore, the Xigaze forearc and Tethyan Himalaya were sutured at ~59 Ma. All three groups of samples are consistent with the Sangdanlin stratigraphy in both their detrital zircon ages and sandstone petrography. Mesozoic Asian-affinity sandstone blocks found along strike in the siliciclastic matrix mélange (Cai et al., 2012; An et al.,

2017; Wang et al., 2017) are conspicuously absent in the Lopu Range region. Metapelite and metabasite blocks in the siliciclastic matrix mélange are lower greenschist facies, indicating that the mélange in the Lopu Range region was not deeply subducted.

The subduction complex which formed along the southern margin of Asia from the early Cretaceous through the Paleocene in the Lopu region is different from other exposures along-strike to the east. Near the Lopu Range, there is no geologic record of upper-plate-derived trench fill entering the trench during subduction of oceanic lithosphere, suggesting that the forearc basin was underfilled and/or separated from the trench by a persistent outer forearc high. The first depositional contact between the Tethyan Himalaya strata and Asian strata is well dated to ~59 Ma (Ding et al., 2005; Wang et al., 2011; DeCelles et al., 2014; Wu et al., 2014; Hu et al., 2015a). A sandstone block of this age in the mélange indicates that the first Tethyan Himalaya strata entered the trench and were incorporated into the siliciclastic matrix mélange at ~59 Ma. As the thickness of Tethyan strata entering the trench increased, the deformation changed from block-in-matrix mélange to imbricate thrusting. In the siliciclastic matrix mélange, blocks of Tethyan Himalaya strata and a block of Asian affinity with a maximum depositional age of ~59 Ma are found amongst blocks of ocean plate stratigraphy kilometers away from the paleo-trench, but it remains unclear whether this apparent mixing was the result of deformation during the final stage of subduction complex formation or during northward folding and thrusting during development of the Lopu Range and the GCT.

Acknowledgements

This research was supported by NSF Continental Dynamics grant EAR-1008527. Analyses were conducted in the Arizona LaserChron Center, which is supported by NSF EAR-1338583. We also thank LaserChron staff members, professor Ding Lin, field assistants Fu Jiajun and Alyssa

Abbey, and Xiumian Hu and three anonymous reviewers for their helpful feedback. This research was supported by additional funding from Chevron Texaco and the Peter J. Coney scholarship fund.

References

Abrajevitch, A.V., Ali, J.R., Aitchison, J.C., Badengzhu, Davis, A.M., Liu, J., and Ziabrev, S.V., 2005, Neotethys and the India–Asia collision: Insights from a palaeomagnetic study of the Dazhuqu ophiolite, southern Tibet: Earth and Planetary Science Letters, v. 233, no. 1-2, p. 87–102, doi: 10.1016/j.epsl.2005.02.003.

Aitchison, J.C., Ali, J.R., and Davis, A.M., 2007, When and where did India and Asia collide?: Journal of Geophysical Research-Solid Earth, v. 112, no. B5, p. 1–19, doi: 10.1029/2006JB004706.

Aitchison, J.C., Badengzhu, Davis, A.M., Liu, J.B., Luo, H., Malpas, J.G., McDermid, I., Wu, H.Y., Ziabrev, S.V., and Zhou, M.F., 2000, Remnants of a Cretaceous intra-oceanic subduction system within the Yarlung-Zangbo suture (southern Tibet): Earth and Planetary Science Letters, v. 183, p. 231–244.

Aitchison, J.C., Davis, A.M., and Luo, H., 2002, New constraints on the India–Asia collision: the Lower Miocene Gangrinboche conglomerates, Yarlung Tsangpo suture zone, SE Tibet: Journal of Asian Earth Sciences.

Aitchison, J.C., Xia, X., Baxter, A.T., and Ali, J.R., 2011, Detrital zircon U-Pb ages along the Yarlung-Tsangpo suture zone, Tibet: Implications for oblique convergence and collision between India and Asia: Gondwana Research, v. 20, no. 4, p. 691–709, doi: 10.1016/j.gr.2011.04.002.

An, W., Hu, X., and Garzanti, E., 2017, Sandstone provenance and tectonic evolution of the Xiukang Mélange from Neotethyan subduction to India–Asia collision (Yarlung-Zangbo suture, south Tibet): Gondwana Research, v. 41, p. 222–234, doi: 10.1016/j.gr.2015.08.010.

An, W., Hu, X., Garzanti, E., Boudagher-Fadel, M., Wang, J., and Sun, G., 2014, Xigaze forearc basin revisited (South Tibet): Provenance changes and origin of the Xigaze Ophiolite: Geological Society of America Bulletin, v. 126, no. 11-12, p. 1595–1613, doi: 10.1130/B31020.1.

Baxter, A.T., Aitchison, J.C., Ali, J.R., Chan, J.S.-L., and Chan, G.H.N., 2016, Detrital chrome spinel evidence for a Neotethyan intra-oceanic island arc collision with India in the Paleocene: Journal of Asian Earth Sciences, v. 128, p. 90–104, doi: 10.1016/j.jseaes.2016.06.023.

Besse, J., and Courtillot, V., 1988, Paleogeographic maps of the continents bordering the Indian

880 Ocean since the Early Jurassic: Journal of Geophysical Research-Solid Earth, v. 93, no. B10,
881 p. 11791–11808, doi: 10.1029/JB093iB10p11791.

882 Burg, J.P., and Chen, G., 1984, Tectonics and structural zonation of southern Tibet, China:
883 Nature, v. 311, no. 5983, p. 219–223, doi: 10.1038/311219a0.

884 Burg, J.P., Leyreloup, A., Girardeau, J., and Chen, G., 1987, Structure and metamorphism of a
885 tectonically thickened continental crust: the Yalu Tsangpo suture zone (Tibet): Philosophical
886 Transactions of the Royal Society of London Series a-Mathematical Physical and
887 Engineering Sciences, v. 321, no. 1557, p. 67–86, doi: 10.1098/rsta.1987.0005.

888 Burg, J.P., Marcoux, J., and Cheng, G., 1985, Wildflysch and Exotic Blocks along the Yarling
889 Zangbo Suture Zone: Age and Geodynamic Significance: Terra Cognita.

890 Cai, F., Ding, L., and Yue, Y., 2011, Provenance analysis of upper Cretaceous strata in the
891 Tethys Himalaya, southern Tibet: Implications for timing of India–Asia collision: Earth and
892 Planetary Science Letters, v. 305, no. 1-2, p. 195–206, doi: 10.1016/j.epsl.2011.02.055.

893 Cai, F., Ding, L., Leary, R.J., Wang, H., Xu, Q., Zhang, L., and Yue, Y., 2012,
894 Tectonostratigraphy and provenance of an accretionary complex within the Yarlung–Zangpo
895 suture zone, southern Tibet: Insights into subduction–accretion processes in the Neo-Tethys:
896 Tectonophysics, v. 574-575, p. 181–192, doi: 10.1016/j.tecto.2012.08.016.

897 Chu, M.-F., Chung, S.-L., Song, B., Liu, D., O'Reilly, S.Y., Pearson, N.J., Jiannqing, J., and
898 Wen, D.-J., 2006, Zircon U-Pb and Hf isotope constraints on the Mesozoic tectonics and
899 crustal evolution of southern Tibet: Geology, v. 34, p. 745–748, doi: 10.1130/G22725.1.

900 Clift, P., and Vannucchi, P., 2004, Controls on tectonic accretion versus erosion in subduction
901 zones: Implications for the origin and recycling of the continental crust: Reviews of
902 Geophysics, v. 42, no. 2, p. 1–31, doi: 10.1029/2003rg000127.

903 Copley, A., Avouac, J.-P., and Royer, J.-Y., 2010, India-Asia collision and the Cenozoic
904 slowdown of the Indian plate: Implications for the forces driving plate motions: Journal of
905 Geophysical Research-Solid Earth, v. 115, no. B3, p. B03410, doi: 10.1029/2009JB006634.

906 Dai, J., Wang, C., Polat, A., Santosh, M., Li, Y., and Ge, Y., 2013, Rapid forearc spreading
907 between 130–120 Ma: Evidence from geochronology and geochemistry of the Xigaze
908 ophiolite, southern Tibet: Lithos,, p. 1–54, doi: 10.1016/j.lithos.2013.03.011.

909 Dai, J., Wang, C., Zhu, D., Li, Y., Zhong, H., and Ge, Y., 2015, Multi-stage volcanic activities
910 and geodynamic evolution of the Lhasa terrane during the Cretaceous: insights from the
911 Xigaze forearc basin: Lithos, v. 218-219, p. 127–140, doi: 10.1016/j.lithos.2015.01.019.

912 Davis, A.M., Aitchison, J.C., Luo, H., and Zyabrev, S., 2002, Paleogene island arc collision-
913 related conglomerates, Yarlung–Tsangpo suture zone, Tibet: Sedimentary Geology, v. 150,
914 no. 3-4, p. 247–273, doi: 10.1016/S0037-0738(01)00199-3.

915 DeCelles, P.G., Kapp, P., Gehrels, G.E., and Ding, L., 2014, Paleocene-Eocene foreland basin

evolution in the Himalaya of southern Tibet and Nepal: Implications for the age of initial India-Asia collision: Tectonics, v. 33, no. 5, p. 824–849, doi: 10.1002/2014TC003522.

DeCelles, P.G., Kapp, P., Quade, J., and Gehrels, G.E., 2011, Oligocene-Miocene Kailas basin, southwestern Tibet: Record of postcollisional upper-plate extension in the Indus-Yarlung suture zone: Geological Society of America Bulletin, v. 123, no. 7-8, p. 1337–1362, doi: 10.1130/B30258.1.

DeCelles, P.G., Robinson, D.M., and Zandt, G., 2002, Implications of shortening in the Himalayan fold-thrust belt for uplift of the Tibetan Plateau: Tectonics, v. 21, no. 6, p. 1–25, doi: 10.1029/2001tc001322.

Dickinson, W.R., 1970, Interpreting Detrital Modes of Graywacke and Arkose: Journal of Sedimentary Research, v. 40, no. 2, p. 695–707, doi: 10.1306/74D72018-2B21-11D7-8648000102C1865D.

Dickinson, W.R., and Gehrels, G.E., 2009, Use of U–Pb ages of detrital zircons to infer maximum depositional ages of strata: A test against a Colorado Plateau Mesozoic database: Earth and Planetary Science Letters, v. 288, p. 115–125, doi: 10.1016/j.epsl.2009.09.013.

Dickinson, W.R., Beard, L.S., Brakenridge, G.R., Erjavec, J.L., Ferguson, R.C., Inman, K.F., Knepp, R.A., Lindberg, F.A., And Ryberg, P.T., 1983, Provenance of North American Phanerozoic sandstones in relation to tectonic setting: Geological Society of America Bulletin, v. 94, no. 2, p. 222–235, doi: 10.1130/0016-7606(1983)94<222:PONAPS>2.0.CO;2.

Ding, L., Kapp, P., and Wan, X.Q., 2005, Paleocene-Eocene record of ophiolite obduction and initial India-Asia collision, south central Tibet: Tectonics, v. 24, no. 3, p. 1–18, doi: 10.1029/2004tc001729.

Du, X., Chen, X., Wang, C., Wei, Y., Li, Y., and Jansa, L., 2015, Geochemistry and detrital zircon U-Pb dating of Lower Cretaceous volcaniclastics in the Babazhadong section, Northern Tethyan Himalaya: Implications for the breakup of Eastern Gondwana: Cretaceous Research, v. 52, p. 127–137, doi: 10.1016/j.cretres.2014.08.002.

Dupuis, C., Hébert, R., Dubois-Côté, V., and Guilmette, C., 2005a, The Yarlung Zangbo Suture Zone ophiolitic mélange (southern Tibet): new insights from geochemistry of ultramafic rocks: Journal of Asian Earth ….

Dupuis, C., Hébert, R., Dubois-Côté, V., Guilmette, C., Wang, C.S., and LI, Z.J., 2006, Geochemistry of sedimentary rocks from mélange and flysch units south of the Yarlung Zangbo suture zone, southern Tibet: Journal of Asian Earth Sciences, v. 26, no. 5, p. 489–508, doi: 10.1016/j.jseaes.2004.11.002.

Dupuis, C., Hébert, R., Dubois-Côté, V., Wang, C.S., LI, Y.L., and LI, Z.J., 2005b, Petrology and geochemistry of mafic rocks from mélange and flysch units adjacent to the Yarlung Zangbo Suture Zone, southern Tibet: Chemical Geology, v. 214, no. 3-4, p. 287–308, doi: 10.1016/j.chemgeo.2004.10.005.

954 Dürr, S.B., 1996, Provenance of Xigaze fore-arc basin clastic rocks (Cretaceous, south Tibet):
955 Geological Society of America Bulletin, v. 108, no. 6, p. 669–684.

956 Einsele, G., Liu, B., Dürr, S., Frisch, W., Liu, G., Luterbacher, H.P., Ratschbacher, L., Ricken,
957 W., Wendt, J., Wetzel, A., Yu, G., and Zheng, H., 1994, The Xigaze forearc basin: evolution
958 and facies architecture (Cretaceous, Tibet): Sedimentary Geology, v. 90, no. 1-2, p. 1–32,
959 doi: 10.1016/0037-0738(94)90014-0.

960 Garzanti, E., 1999, Stratigraphy and sedimentary history of the Nepal Tethys Himalaya passive
961 margin: Journal of Asian Earth Sciences, v. 17, no. 5-6, p. 805–827, doi: 10.1016/S1367-
962 9120(99)00017-6.

963 Gazzi, P., 1966, Le Arenarie del Flysche Sopracretaceo dell'Appennino Modenese: Correlazioni
964 con Flysch di Monghidoro: Mineralogica et Petrographica Acta, v. 12, p. 69–97.

965 Gehrels, G., Kapp, P., DeCelles, P., Pullen, A., Blakey, R., Weislogel, A., Ding, L., Guynn, J.,
966 Martin, A., McQuarrie, N., and Yin, A., 2011, Detrital zircon geochronology of pre-Tertiary
967 strata in the Tibetan-Himalayan orogen: Tectonics, v. 30, no. 5, p. 1–27, doi:
968 10.1029/2011tc002868.

969 Gehrels, G.E., Valencia, V.A., and Ruiz, J., 2008, Enhanced precision, accuracy, efficiency, and
970 spatial resolution of U-Pb ages by laser ablation-multicollector-inductively coupled plasma-
971 mass spectrometry: Geochemistry Geophysics Geosystems, v. 9, no. 3, p. 1–13, doi:
972 10.1029/2007GC001805.

973 Gibbons, A.D., Zahirovic, S., Müller, R.D., Whittaker, J.M., and Yatheesh, V., 2015, A tectonic
974 model reconciling evidence for the collisions between India, Eurasia and intra-oceanic arcs
975 of the central-eastern Tethys: Gondwana Research, v. 28, no. 2, p. 451–492, doi:
976 10.1016/j.gr.2015.01.001.

977 Girardeau, J., Marcoux, J., and Zao, Y., 1984, Lithologic and tectonic environment of the Xigaze
978 ophiolite (Yarlug Zangbo suture zone, Southern Tibet, China), and kinematics of its
979 emplacement: Eclogae Geologicae Helvetiae, v. 77, no. 1, p. 153–170, doi: 10.5169/seals-
980 165503.

981 Guilmette, C., Hébert, R., Dostal, J., Indares, A., Ullrich, T., Bédard, É., and Wang, C., 2012,
982 Discovery of a dismembered metamorphic sole in the Saga ophiolitic mélange, South Tibet:
983 Assessing an Early Cretaceous disruption of the Neo-Tethyan supra-subduction zone and
984 consequences on basin closing: Gondwana Research, v. 22, no. 2, p. 398–414, doi:
985 10.1016/j.gr.2011.10.012.

986 Guilmette, C., Hébert, R., Wang, C., and Villeneuve, M., 2009, Geochemistry and
987 geochronology of the metamorphic sole underlying the Xigaze Ophiolite, Yarlung Zangbo
988 Suture Zone, South Tibet: Lithos, v. 112, no. 1-2, p. 149–162, doi:
989 10.1016/j.lithos.2009.05.027.

990 Guo, L., Liu, Y., Liu, S., Cawood, P.A., Wang, Z., and Liu, H., 2013, Petrogenesis of Early to
991 Middle Jurassic granitoid rocks from the Gangdese belt, Southern Tibet: Implications for

early history of the Neo-Tethys: Lithos, v. 179, p. 320–333, doi: 10.1016/j.lithos.2013.06.011.

Heim, A., and Gansser, A., 1939, Central Himalaya:.

Hébert, R., Bezard, R., Guilmette, C., Dostal, J., Wang, C.S., and Liu, Z.F., 2012, The Indus–Yarlung Zangbo ophiolites from Nanga Parbat to Namche Barwa syntaxes, southern Tibet: First synthesis of petrology, geochemistry, and geochronology with incidences on geodynamic reconstructions of Neo-Tethys: Gondwana Research, v. 22, no. 2, p. 377–397, doi: 10.1016/j.gr.2011.10.013.

van Hinsbergen, D.J.J., Kapp, P., Dupont-Nivet, G., Lippert, P.C., DeCelles, P.G., and Torsvik, T.H., 2011b, Restoration of Cenozoic deformation in Asia and the size of Greater India: Tectonics, v. 30, doi: 10.1029/2011tc002908.

van Hinsbergen, D.J.J., Lippert, P.C., Dupont-Nivet, G., McQuarrie, N., Doubrovine, P.V., Spakman, W., and Torsvik, T.H., 2012, Greater India Basin hypothesis and a two-stage Cenozoic collision between India and Asia: Proceedings of the National Academy of Sciences, v. 109, no. 20, p. 7659–7664, doi: 10.1073/pnas.1117262109.

van Hinsbergen, D.J.J., Steinberger, B., Doubrovine, P.V., and Gassmoller, R., 2011a, Acceleration and deceleration of India-Asia convergence since the Cretaceous: Roles of mantle plumes and continental collision: Journal of Geophysical Research-Solid Earth, v. 116, doi: 10.1029/2010jb008051.

Hu, X., Garzanti, E., and An, W., 2015c, Provenance and drainage system of the Early Cretaceous volcanic detritus in the Himalaya as constrained by detrital zircon geochronology: Journal of Paleogeography, v. 4, no. 1, p. 85–98, doi: 10.3724/SP.J.1261.2015.00069.

Hu, X., Garzanti, E., Moore, T., and Raffi, I., 2015a, Direct stratigraphic dating of India-Asia collision onset at the Selandian (middle Paleocene, 59 ± 1 Ma): Geology,, p. 1–4, doi: 10.1130/G36872.1.

Hu, X., Garzanti, E., Wang, J., Huang, W., An, W., and Webb, A., 2016, The timing of India-Asia collision onset – Facts, theories, controversies: Earth-Science Reviews, v. 160, no. C, p. 264–299, doi: 10.1016/j.earscirev.2016.07.014.

Hu, X., Sinclair, H.D., Wang, J., Jiang, H., and Wu, F., 2012, Late Cretaceous-Palaeogene stratigraphic and basin evolution in the Zhepure Mountain of southern Tibet: implications for the timing of India-Asia initial collision: Basin Research, v. 24, no. 5, p. 520–543, doi: 10.1111/j.1365-2117.2012.00543.x.

Hu, X., Wang, J., Boudagher-Fadel, M., Garzanti, E., and An, W., 2015b, New insights into the timing of the India-Asia collision from the Paleogene Quxia and Jialazi Formations of the Xigaze forearc basin, South Tibet: Gondwana Research,, p. 1–60, doi: 10.1016/j.gr.2015.02.007.

Hu, X.M., Jansa, L., Chen, L., Griffin, W.L., O'Reilly, S.Y., and al, E., 2010, Provenance of Lower Cretaceous Wölong volcaniclastics in the Tibetan Tethyan Himalaya: Implications for the final breakup of eastern Gondwana: Sedimentary Geology, v. 223, no. 3-4, p. 193–205, doi: 10.1016/j.sedgeo.2009.11.00810.1016/j.sedgeo.2009.11.008.

Huang, W., van Hinsbergen, D.J.J., Maffione, M., Orme, D.A., Dupont-Nivet, G., Guilmette, C., Ding, L., Guo, Z., and Kapp, P., 2015, Lower Cretaceous Xigaze ophiolites formed in the Gangdese forearc: Evidence from paleomagnetism, sediment provenance, and stratigraphy: Earth and Planetary Science Letters, v. 415, no. C, p. 142–153, doi: 10.1016/j.epsl.2015.01.032.

von Huene, R., and Scholl, D.W., 1991, Observations at convergent margins concerning sediment subduction, subduction erosion, and the growth of continental-crust: Reviews of Geophysics, v. 29, no. 3, p. 279–316, doi: 10.1029/91RG00969.

von Huene, R., Ranero, C.R., and Vannucchi, P., 2004, Generic model of subduction erosion: Geology, v. 32, no. 10, p. 913–916, doi: 10.1130/g20563.1.

Huot, F., Hébert, R., Varfalvy, V., and Beaudoin, G., 2002, The Beimarang mélange (southern Tibet) brings additional constraints in assessing the origin, metamorphic evolution and obduction processes of the Yarlung Zangbo ophiolite: Journal of Asian Earth Sciences.

Ingersoll, R.V., Bullard, T.F., Ford, R.L., Grimm, J.P., Pickle, J.D., and Sares, S.W., 1984, The Effect of Grain Size on Detrital Modes: A Test of the Gazzi-Dickinson Point-Counting Method: Journal of Sedimentary Research, v. 54, no. 1, p. 103–116, doi: 10.1306/212F83B9-2B24-11D7-8648000102C1865D.

Isozaki, Y., Maruyama, S., and Furuoka, F., 1990, Accreted oceanic materials in Japan: Tectonophysics.

Jadoul, F., Berra, F., and Garzanti, E., 1998, The Tethys Himalayan passive margin from Late Triassic to Early Cretaceous (South Tibet): Journal of Asian Earth Sciences, v. 16, no. 2-3, p. 173–194, doi: 10.1016/S0743-9547(98)00013-0.

Ji, W.-Q., Wu, F.-Y., Chung, S.-L., Li, J.-X., and Liu, C.-Z., 2009, Zircon U–Pb geochronology and Hf isotopic constraints on petrogenesis of the Gangdese batholith, southern Tibet: Chemical Geology, v. 262, no. 3-4, p. 229–245, doi: 10.1016/j.chemgeo.2009.01.020.

Jin, X., Huang, H., Shi, Y., and Zhan, L., 2015, Origin of Permian exotic limestone blocks in the Yarlung Zangbo Suture Zone, Southern Tibet, China: With biostratigraphic, sedimentary and regional geological constraints: Journal of Asian Earth Sciences, v. 104, p. 22–38, doi: 10.1016/j.jseaes.2014.07.036.

Kang, Z.-Q., Xu, J.-F., Wilde, S.A., Feng, Z.-H., Chen, J.-L., Wang, B.-D., Fu, W.-C., and Pan, H.-B., 2014, Geochronology and geochemistry of the Sangri Group Volcanic Rocks, Southern Lhasa Terrane: Implications for the early subduction history of the Neo-Tethys and Gangdese Magmatic Arc: Lithos, v. 200-201, no. C, p. 157–168, doi: 10.1016/j.lithos.2014.04.019.

1067 Kusky, T.M., Windley, B.F., Safonova, I., and Wakita, K., 2013, Recognition of ocean plate
1068 stratigraphy in accretionary orogens through Earth history: A record of 3.8billion years of
1069 sea floor spreading, subduction, and accretion: Gondwana Research, v. 24, no. 2, p. 501–
1070 547, doi: 10.1016/j.gr.2013.01.004.

1071 Laskowski, A.K., Kapp, P., Ding, L., Campbell, C., and Liu, X., 2017, Tectonic evolution of the
1072 Yarlung suture zone, Lopu Range region, southern Tibet: Tectonics, v. 36, no. 1, p. 108–136,
1073 doi: 10.1002/2016TC004334.

1074 Laskowski, A.K., Kapp, P., Vervoort, J.D., and Ding, L., 2016, High-pressure Tethyan Himalaya
1075 rocks along the India-Asia suture zone in southern Tibet: Lithosphere, v. 8, no. 5, p. 574–
1076 582, doi: 10.1130/L544.1.

1077 Leary, R., Orme, D.A., Laskowski, A.K., DeCelles, P.G., Kapp, P., Carrapa, B., and Dettinger,
1078 M., 2016a, Along-strike diachroneity in deposition of the Kailas Formation in central
1079 southern Tibet: Implications for Indian slab dynamics: Geosphere, v. 12, no. 4, p. 1–26, doi:
1080 10.1130/GES01325.1.

1081 Leary, R.J., DeCelles, P.G., Quade, J., Gehrels, G.E., and Waanders, G., 2016b, The Liuqu
1082 Conglomerate, southern Tibet: Early Miocene basin development related to deformation
1083 within the Great Counter Thrust system: Lithosphere, v. 8, no. 5, p. 427–450, doi:
1084 10.1130/L542.1.

1085 Lee, H.-Y., Chung, S.-L., Lo, C.-H., Jiannqing, J., Lee, T.-Y., Qian, Q., and Zhang, Q., 2009,
1086 Eocene Neotethyan slab breakoff in southern Tibet inferred from the Linzizong volcanic
1087 record: Tectonophysics, v. 477, p. 20–35, doi: 10.1016/j.tecto.2009.02.031.

1088 Li, C., Hu, J., Zhai, Q.-G., and Dong, Y., 2007, New evidence of collision and collision time
1089 between India and Asia: Geological Bulletin of China, v. 26, no. 10, p. 1299–1303.

1090 Li, G., Kohn, B., Sandiford, M., Xu, Z., and Wei, L., 2015a, Constraining the age of Liuqu
1091 Conglomerate, southern Tibet: Implications for evolution of the India–Asia collision zone:
1092 Earth and Planetary Science Letters, v. 426, p. 259–266, doi: 10.1016/j.epsl.2015.06.010.

1093 Li, G., Sandiford, M., Boger, S., Liu, X., and Wei, L., 2015b, Provenance of the Upper
1094 Cretaceous to Lower Tertiary Sedimentary Relicts in the Renbu Mélange Zone, within the
1095 Indus-Yarlung Suture Zone: The Journal of Geology, v. 123, no. 1, p. 39–54, doi:
1096 10.1086/680207?ref=no-x-route:f9fa42b40529df98fc7109d33c73e439.

1097 Li, J., Hu, X., Garzanti, E., An, W., and Wang, J., 2015c, Paleogene carbonate microfacies and
1098 sandstone provenance (Gamba area, South Tibet): Stratigraphic response to initial India-Asia
1099 continental collision: Journal of Asian Earth Sciences, v. 104, p. 39–54, doi:
1100 10.1016/j.jseaes.2014.10.027.

1101 Li, Y., Wang, C., Dai, J., Xu, G., Hou, Y., and Li, X., 2015d, Propagation of the deformation and
1102 growth of the Tibetan-Himalayan orogen: A review: Earth-Science Reviews, v. 143, p. 36–
1103 61, doi: 10.1016/j.earscirev.2015.01.001.

1104 Liu, C.J., Yin, J.X., Sun, X.X., and Sun, Y.Y., 1988, Marine Late Cretaceous–Early Tertiary
1105 sequences: The non-flysch deposits of the Xigaze forearc basin in south Xizang: J. Inst.
1106 Geol. Chin. Acad. Sci, v. 3, p. 130–157.

1107 Liu, G., and Einsele, G., 1994, Sedimentary history of the Tethyan basin in the Tibetan
1108 Himalayas: International Journal of Earth Sciences, v. 83, no. 1, p. 32–61, doi:
1109 10.1007/BF00211893.

1110 Liu, G., and Einsele, G., 1996, Various types of olistostromes in a closing ocean basin, Tethyan
1111 Himalaya (Cretaceous, Tibet): Sedimentary Geology, v. 104, no. 1-4, p. 203–226, doi:
1112 10.1016/0037-0738(95)00129-8.

1113 Liu, J., and Aitchison, J.C., 2002, Upper Paleocene radiolarians from the Yamdrok mélange,
1114 south Xizang (Tibet), China: Micropaleontology, v. 48, p. 145–154.

1115 Ludwig, K., and Mundil, R., 2002, Extracting reliable U-Pb ages and errors from complex
1116 populations of zircons from Phanerozoic tuffs: 12th Goldschmidt Conference.

1117 Maffione, M., van Hinsbergen, D.J.J., Koornneef, L.M.T., Guilmette, C., Hodges, K.V.,
1118 Borneman, N., Huang, W., Ding, L., and Kapp, P., 2015, Forearc hyperextension
1119 dismembered the south Tibetan ophiolites: Geology, v. 43, no. 6, p. 475–478, doi:
1120 10.1130/G36472.1.

1121 Marcoux, J., De Wever, P., Nicolas, A., Girardeau, J., Xiao, X., Fa, C., Cao, Y., Wang, N.,
1122 Bassoullet, J.P., Colchen, M., and Mascle, G., 1982, Preliminary report of depositional
1123 sediments on top of volcanic member: Xigaze ophiolite (Yarlung Zangbo Suture Zone);
1124 South Xigang (Tibet): Ofioliti, v. 2/3, p. 395–396.

1125 Meng, Y., Dong, H., Cong, Y., Xu, Z., and Cao, H., 2016, The early-stage evolution of the Neo-
1126 Tethys Ocean: Evidence from granitoids in the middle Gangdese batholith, southern Tibet:
1127 Journal of Geodynamics, v. 94-95, p. 34–49, doi: 10.1016/j.jog.2016.01.003.

1128 Molnar, P., and Stock, J.M., 2009, Slowing of India's convergence with Eurasia since 20 Ma and
1129 its implications for Tibetan mantle dynamics: Tectonics, v. 28, no. 3, doi:
1130 10.1029/2008TC002271.

1131 Molnar, P., and Tapponnier, P., 1975, Cenozoic Tectonics of Asia: Effects of a Continental
1132 Collision: Science, v. 189, no. 4201, p. 419–426, doi: 10.1126/science.189.4201.419.

1133 Murphy, M.A., and Yin, A., 2003, Structural evolution and sequence of thrusting in the Tethyan
1134 fold-thrust belt and Indus-Yalu suture zone, southwest Tibet: Geological Society of America
1135 Bulletin, v. 115, no. 1, p. 21–34, doi: 10.1130/0016-
1136 7606(2003)115<0021:SEASOT>2.0.CO;2.

1137 Najman, Y., Appel, E., Boudagher-Fadel, M., Bown, P., Carter, A., Garzanti, E., Godin, L., Han,
1138 J., Liebke, U., Oliver, G., Parrish, R., and Vezzoli, G., 2010, Timing of India-Asia collision:
1139 Geological, biostratigraphic, and palaeomagnetic constraints: Journal of Geophysical
1140 Research-Solid Earth, v. 115, no. B12, p. 1–18, doi: 10.1029/2010JB007673.

1141 Nicolas, A., Girardeau, J., Marcoux, J., Dupre, B., Xibin, W., Yougong, C., Haixiang, Z., and
1142 XUCHANG, X., 1981, The Xigaze ophiolite (Tibet): a peculiar oceanic lithosphere: Nature,
1143 v. 294, no. 5840, p. 414–417, doi: 10.1038/294414a0.

1144 Orme, D.A., and Laskowski, A.K., 2016, Basin Analysis of the Albian–Santonian Xigaze
1145 Forearc, Lazi Region, South-Central Tibet: Journal of Sedimentary Research, v. 86, no. 8, p.
1146 894–913, doi: 10.2110/jsr.2016.59.

1147 Orme, D.A., Carrapa, B., and Kapp, P., 2015, Sedimentology, Provenance And Geochronology
1148 Of The Upper Cretaceous-Lower Eocene Western Xigaze Forearc Basin, Southern Tibet:
1149 Basin Research, v. 27, no. 4, p. 387–411, doi: 10.1111/bre.12080.

1150 Painter, C.S., Carrapa, B., DeCelles, P.G., Gehrels, G.E., and Thomson, S.N., 2014, Exhumation
1151 of the North American Cordillera revealed by multi-dating of Upper Jurassic-Upper
1152 Cretaceous foreland basin deposits: Geological Society of America Bulletin,, p. 1–27, doi:
1153 10.1130/B30999.1.

1154 Patriat, P., and Achache, J., 1984, India–Eurasia collision chronology has implications for crustal
1155 shortening and driving mechanism of plates: Nature, v. 311, no. 5987, p. 615–621, doi:
1156 10.1038/311615a0.

1157 Patzelt, A., Li, H., Wang, J., and Appel, E., 1996, Palaeomagnetism of Cretaceous to Tertiary
1158 sediments from southern Tibet: evidence for the extent of the northern margin of India prior
1159 to the collision with Eurasia: Tectonophysics, v. 259, no. 4, p. 259–284, doi: 10.1016/0040-
1160 1951(95)00181-6.

1161 Quidelleur, X., Grove, M., Lovera, O.M., Harrison, T.M., Yin, A., and Ryerson, F.J., 1997,
1162 Thermal evolution and slip history of the Renbu Zedong Thrust, southeastern Tibet: Journal
1163 of Geophysical Research-Solid Earth, v. 102, no. B2, p. 2659–2679, doi:
1164 10.1029/96JB02483.

1165 Ratschbacher, L., Frisch, W., Liu, G., and Chen, C., 1994, Distributed deformation in southern
1166 and western Tibet during and after the India-Asia collision: Journal of Geophysical
1167 Research-Solid Earth, v. 99, no. B10, p. 19917–19945, doi: 10.1029/94JB00932.

1168 Searle, M.P., Windley, B.F., Coward, M.P., Cooper, D., Rex, A.J., Rex, D., Li, T., Xiao, X., Jan,
1169 M.Q., Thakur, V.C., and Kumar, S., 1987, The closing of Tethys and the tectonics of the
1170 Himalaya: Geological Society of America Bulletin, v. 98, p. 678–701, doi: 10.1130/0016-
1171 7606(1987)98<678:TCOTAT>2.0.CO;2.

1172 Shackleton, R.M., 1981, Structure of Southern Tibet: report on a traverse from Lhasa to
1173 Khatmandu organised by Academia Sinica: Journal of Structural Geology, v. 3, no. 1, p. 97–
1174 105, doi: 10.1016/0191-8141(81)90060-2.

1175 Stern, C.R., 2011, Subduction erosion: Rates, mechanisms, and its role in arc magmatism and the
1176 evolution of the continental crust and mantle: Gondwana Research, v. 20, no. 2-3, p. 284–
1177 308, doi: 10.1016/j.gr.2011.03.006.

Tapponnier, P., Mercier, J.L., Proust, F., Andrieux, J., Armijo, R., Bassoullet, J.P., Brunel, M., Burg, J.P., Colchen, M., Dupre, B., Girardeau, J., Marcoux, J., Mascle, G., Matte, P., et al., 1981, The Tibetan side of the India–Eurasia collision: Nature, v. 294, p. 405–410, doi: 10.1038/294405a0.

Wahrhaftig, C., 1984, Structure of the Marin Headlands Block, California: A Progress Report (M. C. Blake Jr, Ed.): Franciscan Geology of Northern California: Pacific Section S.E.P.M, v. 43, p. 31–50.

Wakita, K., 2015, OPS mélange: a new term for mélanges of convergent margins of the world: International Geology Review, v. 57, no. 5-8, p. 529–539, doi: 10.1080/00206814.2014.949312.

Wakita, K., and Metcalfe, I., 2005, Ocean plate stratigraphy in East and Southeast Asia: Journal of Asian Earth Sciences, v. 24, no. 6, p. 679–702, doi: 10.1016/j.jseaes.2004.04.004.

Wang, C., Li, X., Liu, Z., Li, Y., Jansa, L., Dai, J., and Wei, Y., 2012, Revision of the Cretaceous–Paleogene stratigraphic framework, facies architecture and provenance of the Xigaze forearc basin along the Yarlung Zangbo suture zone: Gondwana Research, v. 22, no. 2, p. 415–433, doi: 10.1016/j.gr.2011.09.014.

Wang, H., Ding, L., Cai, F., Xu, Q., Li, S., Fu, J., Lai, Q., Yue, Y., and Li, X., 2017, Early Tertiary deformation of the Zhongba-Gyangze Thrust in central southern Tibet: Gondwana Research, v. 41, p. 235–248, doi: 10.1016/j.gr.2015.02.017.

Wang, J., Hu, X., Jansa, L., and Huang, Z., 2011, Provenance of the Upper Cretaceous–Eocene Deep-Water Sandstones in Sangdanlin, Southern Tibet: Constraints on the Timing of Initial India-Asia Collision: The Journal of Geology, v. 119, no. 3, p. 293–309, doi: 10.1086/659145.

Wang, J.-G., Hu, X.-M., Boudagher-Fadel, M., Wu, F.-Y., and Sun, G.-Y., 2015, Early Eocene sedimentary recycling in the Kailas area, southwestern Tibet: implications for the initial India-Asia collision: Sedimentary Geology, v. 315, p. 1–13, doi: 10.1016/j.sedgeo.2014.10.009.

Wang, J.G., Hu, X.M., Wu, F.Y., and Jansa, L., 2010, Provenance of the Liuqu Conglomerate in southern Tibet: A Paleogene erosional record of the Himalayan-Tibetan orogen: Sedimentary Geology, v. 231, no. 3-4, p. 74–84, doi: 10.1016/J.Sedgeo.2010.09.004.

Wei, L., Liu, X., Yan, F., Mai, X., Li, G., Liu, X., and Zhou, X., 2011, Palynological evidence sheds new light on the age of the Liuqu Conglomerates in Tibet and its geological significance: Science China Earth Sciences, v. 54, no. 6, p. 901–911, doi: 10.1007/s11430-010-4149-y.

Wen, D.R., Liu, D., Chung, S.L., Chu, M.F., Ji, J., and Zhang, Q., 2008, Zircon SHRIMP U–Pb ages of the Gangdese Batholith and implications for Neotethyan subduction in southern Tibet: Chemical Geology, v. 252, p. 191–201, doi: 10.1016/j.chemgeo.2008.03.003.

Willems, H., and Zhang, B., 1993, Cretaceous and Lower Tertiary sediments of the Tethys Himalaya in the area of Gamba (South Tibet, PR China), *in* Geoscientific investigations in the Tethyan Himalayas, Ber FB Geowiss Univ Bremen, p. 3–27.

Willems, H., Zhou, Z., Zhang, B., and Gräfe, K.U., 1996, Stratigraphy of the upper cretaceous and lower tertiary strata in the Tethyan Himalayas of Tibet (Tingri area, China): Geologische Rundschau, v. 85, p. 723–754.

Wu, F.Y., Ji, W.Q., Liu, C.Z., and Chung, S.L., 2010, Detrital zircon U-Pb and Hf isotopic data from the Xigaze fore-arc basin: Constraints on Transhimalayan magmatic evolution in southern Tibet: Chemical Geology, v. 271, no. 1-2, p. 13–25, doi: 10.1016/J.Chemgeo.2009.12.007.

Wu, F.Y., Ji, W.Q., Wang, J.G., Liu, C.Z., Chung, S.L., and Clift, P.D., 2014, Zircon U-Pb and Hf isotopic constraints on the onset time of India-Asia collision: American Journal of Science, v. 314, no. 2, p. 548–579, doi: 10.2475/02.2014.04.

XBGMR, 1979, Regional Geology Report of the People's Republic of China: 1:1,000,000 (Xigaze H-45, Yadong G-45):, 230 p.

Yang, B., Bi, Z., Zhang, W., Zhang, Y., and Zhang, Z., 2003, Geological map of Saga region:.

Yin, A., and Harrison, T.M., 2000, Geologic evolution of the Himalayan-Tibetan orogen: Annual Review of Earth and Planetary Sciences, v. 28, p. 211–280, doi: 10.1146/annurev.earth.28.1.211.

Yin, A., Harrison, T.M., Murphy, M.A., Grove, M., Nie, S., Ryerson, F.J., Feng, W., and Le, C., 1999, Tertiary deformation history of southeastern and southwestern Tibet during the Indo-Asian collision: Geological Society, v. 111, no. 11, p. 1644–1664, doi: 10.1130/0016-7606(1999)111<1644:TDHOSA>2.3.CO;2.

Yin, A., Harrison, T.M., Ryerson, F.J., Chen, W., Kidd, W.S.F., and Copeland, P., 1994, Tertiary structural evolution of the Gangdese thrust system, southeastern Tibet: Journal of Geophysical Research, v. 99, no. B9, p. 18175–18201, doi: 10.1029/94JB00504.

Yin, J., and Sun, Y., 1988, The Triassic system of the Zhongbei area, Lhaze county, south Tibet: Journal of Institute Geology Chinese Academy Sciences, v. 3, p. 73–79.

Zhang, Q., Willems, H., Ding, L., Gräfe, K.-U., and Appel, E., 2012, Initial India-Asia Continental Collision and Foreland Basin Evolution in the Tethyan Himalaya of Tibet: Evidence from Stratigraphy and Paleontology: The Journal of Geology, v. 120, no. 2, p. 175–7189, doi: 10.1086/663876.

Zhu, B., Kidd, W.S.F., Rowley, D.B., Currie, B.S., and Shafique, N., 2005, Age of Initiation of the India-Asia Collision in the East-Central Himalaya: The Journal of Geology, v. 113, no. 3, p. 265–285, doi: 10.1086/428805.

Zhu, D.C., Zhao, Z.D., Niu, Y., Mo, X.X., and Chung, S.L., 2011, The Lhasa Terrane: Record of

a microcontinent and its histories of drift and growth: Earth and Planetary Science Letters, v. 301, p. 241–255, doi: 10.1016/j.epsl.2010.11.005.

Ziabrev, S.V., Aitchison, J.C., Abrajevitch, A.V., Badengzhu, Davis, A.M., and Luo, H., 2003, Precise radiolarian age constraints on the timing of ophiolite generation and sedimentation in the Dazhuqu terrane, Yarlung-Tsangpo suture zone, Tibet: Journal of the Geological Society, v. 160, p. 591–599.

Supplementary data

1. Detrital zircon U-Pb ages

2. Microprobe analyses

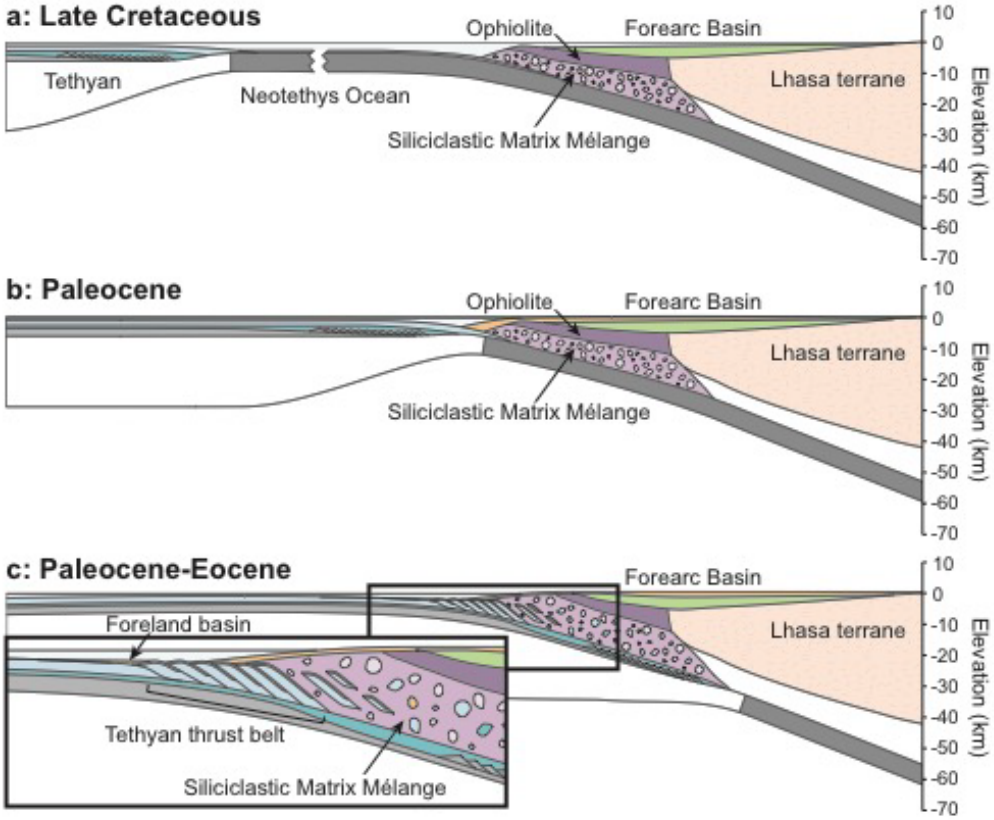

Graphical Abstract